Pergamon

Geochimica et Cosmochimica Acta, Vol. 67, No. 24, pp. 4823–4848, 2003

0016-7037/03 $30.00 + .00

doi:10.1016/j.gca.2003.07.019

Presolar diamond, silicon carbide, and graphite in carbonaceous chondrites: Implications for thermal processing in the solar nebula

GARY R. HUSS,[1,2,*] ALEX P. MESHIK,[3] JULIE B. SMITH,[1] and C. M. HOHENBERG[3]

[1]Department of Geological Sciences, Arizona State University, Tempe, AZ 85287-1404, USA
[2]Center for Meteorite Studies, Arizona State University, Tempe, AZ 85287-1404, USA
[3]McDonnell Center for the Space Sciences and Department of Physics, Washington University, St. Louis, MO 63130, USA

(*Received February* 10, 2003; *accepted in revised form July* 25, 2003)

Abstract—We have determined abundances of presolar diamond, silicon carbide, graphite, and Xe-P1 (Q-Xe) in eight carbonaceous chondrites by measuring the abundances of noble gas tracers in acid residues. The meteorites studied were Murchison (CM2), Murray (CM2), Renazzo (CR2), ALHA77307 (CO3.0), Colony (CO3.0), Mokoia ($CV3_{ox}$), Axtell ($CV3_{ox}$), and Acfer 214 (CH). These data and data obtained previously by Huss and Lewis (1995) provide the first reasonably comprehensive database of presolar-grain abundances in carbonaceous chondrites. Evidence is presented for a currently unrecognized Ne-E(H) carrier in CI and CM2 chondrites.

After accounting for parent-body metamorphism, abundances and characteristics of presolar components still show large variations across the classes of carbonaceous chondrites. These variations correlate with the bulk compositions of the host meteorites and imply that the same thermal processing that was responsible for generating the compositional differences between the various chondrite groups also modified the initial presolar-grain assemblages. The CI chondrites and CM2 matrix have the least fractionated bulk compositions relative to the sun and the highest abundances of most types of presolar material, particularly the most fragile types, and thus are probably most representative of the material inherited from the sun's parent molecular cloud. The other classes can be understood as the products of various degrees of heating of bulk molecular cloud material in the solar nebula, removing the volatile elements and destroying the most fragile presolar components, followed by chondrule formation, metal-silicate fractionation in some cases, further nebula processing in some cases, accretion, and parent body processing. If the bulk compositions and the characteristics of the presolar-grain assemblages in various chondrite classes reflect the same processes, as seems likely, then differential condensation from a nebula of solar composition is ruled out as the mechanism for producing the chondrite classes. Presolar grains would have been destroyed if the nebula had been completely vaporized. Our analysis shows that carbonaceous chondrites reflect all stages of nebular processing and thus are no more closely related to one another than they are to ordinary and enstatite chondrites. *Copyright © 2003 Elsevier Ltd*

1. INTRODUCTION

Presolar grains were incorporated into all classes of chondrites and survive today in the most primitive members of each class (Huss and Lewis, 1995; Huss, 1997). Known types of presolar materials include carbonaceous phases such as diamond, silicon carbide, graphite, and, probably, organic materials, as well as silicon nitride and oxide phases such as corundum, spinel, and hibonite (Lewis et al., 1987; Tang and Anders, 1988; Amari et al., 1990; Hutcheon et al., 1994; Huss et al., 1994; Nittler et al., 1994, 1995, 1997; Choi et al., 1998, 1999). Most recently, presolar silicates were identified in interplanetary dust particles (Messenger et al., 2003). Because these recognized types of presolar grains do not add up to the bulk composition of the solar system, it is clear that they constitute only a small fraction of the presolar matter that provided the building blocks for the solar system.

The known types of presolar material have different thermal and chemical resistance. If all types of chondrites inherited the same initial mixture of presolar grains, then the abundances patterns found in the meteorites today would be expected to reflect the thermal and chemical history of the host meteorites. Good correlations between the abundance patterns within a meteorite class and the petrologic type of the host meteorites show that this expectation is largely satisfied (e.g., Huss, 1990; Huss and Lewis, 1995). Presolar diamonds contain three isotopically distinct noble gas components (P3, HL, and P6) that are released at different temperatures, both in the laboratory and in nature (Huss and Lewis, 1994a, 1994b). The carriers of these components have not been effectively separated in the laboratory and show no evidence of being separable in nature except by thermal destruction (Huss and Lewis, 1994a). Thus these components provide independent evidence about the history of the host material. The abundance of the P3 component, which is released at low temperatures, seems to be a function only of the maximum temperature experienced by the diamond and thus is independent of the nature of the surroundings (Huss and Lewis, 1994b). In contrast, the P6 component releases its xenon only at very high temperatures and thus can serve as a tracer of the original diamond abundance in thermally processed material. The relative abundances of the three noble gas components in diamonds within a class also correlate well with other indicators of the metamorphic grade of the host meteorite (Huss and Lewis, 1994b).

The metamorphism model works well within a chondrite class, but comparisons of the least metamorphosed samples of

* Author to whom correspondence should be addressed (gary.huss@asu.edu).

each class show that the different classes of chondrites did not inherit the same initial mixture of presolar grains. For example, the least metamorphosed CV3 chondrites (e.g., Leoville and Vigarano) and the least metamorphosed EH chondrite (Qingzhen) show abundance patterns for presolar grains and noble-gas characteristics of diamonds that indicate significant heating, but the diamond abundances are quite high and the abundances of the most thermally resistant component in the diamonds (Xe-P6) is significantly higher than in the supposed CI-chondrite-like starting material (Huss and Lewis, 1995). These observations led Huss and Lewis (1995) to postulate that the presolar grains in the CV and EH chondrites were recording preaccretionary thermal processing. In this paper, we investigate the abundances and characteristics of presolar grains from CI and CM2 chondrites and some of the least metamorphosed members of the CR, CH, CO, and CV chondrites. The goal is to identify characteristics of the presolar-grain assemblage in each class that could be indicators of preaccretionary nebular processing. We also investigate the bulk compositional characteristics of each meteorite class to follow up the suggestion by Huss and Lewis (1995) that the abundances and characteristics of presolar grains correlate with the bulk compositional properties of the host meteorites. The implications of such a correlation would be profound, because it would imply that the bulk composition of each chondrite class and the modified suite of presolar grains originated from the same nebular processing. If this were true, then nebula-scale vaporization and recondensation of presolar dust cannot be responsible for the bulk chemical properties of chondrites because the presolar grains would have been destroyed (once vaporized they cannot come back). Instead, thermal processing in the nebula of the bulk dust inherited from the sun's parent molecular cloud is implicated, with the known types of presolar grains providing direct evidence of this processing while the bulk compositions provide information about the majority of the presolar material, the nature of which has not yet been determined.

Huss and Lewis (1995) demonstrated that abundances of presolar diamond, silicon carbide, and graphite can be estimated from lightly processed acid residues of bulk meteorite by means of noble-gas tracers. Diamond abundances can be accurately estimated from HF-HCl residues that have been "etched" by an oxidant (e.g., chromic acid, nitric acid) to remove the dominant planetary gas component in the meteorite by measuring the Xe-HL content of the residue and of the diamond separate from the same meteorite. If the acid residues are prepared using high-yield procedures, these abundance estimates are accurate to ~10%, with the main uncertainties being small sample losses associated with preparing the etched residue and the noble gas abundances in the samples (Huss and Lewis, 1995). Silicon carbide abundances can be estimated from Ne-E(H) in the etched residues. We did not prepare silicon carbide separates because this is quite difficult to do. Instead we used the Ne-E(H) content for silicon carbide from Murchison separates prepared by Amari et al. (1994) to estimate the silicon carbide content in the meteorite. Thus, these abundance estimates are less accurate than those for presolar diamond, but should still be reliable at the ~20% level (Huss and Lewis, 1995). Graphite abundances can be estimated from Ne-E(L) in the etched residues. However, Huss and Lewis (1995) found that some Ne-E(L) is lost during etching. In addition, the Ne-E(L) content of presolar graphite is not known with any certainty because graphite separates prepared by Amari et al. (1994) contain both isotopically anomalous (presolar) and isotopically normal (presumably of local origin) graphite (Zinner et al., 1995). Thus the true graphite abundances in chondrites are poorly known, but comparisons of Ne-E(L) content in a series of etched residues processed the same way can be used to estimate relative abundances among meteorites.

In this paper, we present noble gas data for HF-HCl residues, chromic-acid-etched residues, and diamond separates from eight meteorites from five classes of carbonaceous chondrites (CM2, CR2, CV3, CO3, and CH). These data are then converted to abundance information for diamond, silicon carbide, and graphite in the meteorites. The residues were prepared using the high-yield methods of Huss and Lewis (1995). The data for CI, CV3, and CO3 chondrites from Huss and Lewis (1995) and the new data presented in this paper provide the first consistent set of abundance data for the carbonaceous chondrites. The abundance data and the noble gas data for diamond separates are evaluated in the context of the petrography and the bulk compositions of the host chondrites and reveal some significant insights into the preaccretionary history of the meteorites and the relationships between them. The combined data show that carbonaceous chondrites span the range from the least processed material available for study (CI chondrites and CM2 matrix) to some of the most highly processed material known in chondrites (CV chondrites). Thus, carbonaceous chondrites are not closely related and should not be considered as a group that is distinct from ordinary or enstatite chondrites.

Table 1. Meteorite samples processed for this study.

Meteorite	Class	Sample wt. (g)	Nature of sample	Source
Murchison	CM2	2.03	Crust-free chips	1
Murray	CM2	2.69	Crust-free chips	1
Renazzo	CM2	1.88	Cut end piece	2
Axtell	CV3	8.40	Unpolished part slice	3
Mokoia	CV3	2.75	Crust-free chips	1
Colony	CO3	2.34	Part of polished slice	1
ALHA77307	CO3	1.34	Crust-free chips	4
Acfer 214	CH	4.50	Part of polished slice	3

(1) Center for Meteorite Studies, Arizona State University. (2) Naturhistorisches Museum, Vienna. (3) Collection of G. J. Wasserburg, California Institute of Technology. (4) Antarctic Meteorite Curatorial Facility, Johnson Space Center.

2. EXPERIMENTAL

2.1. Sample Selection

The details of the samples used in this study are given in Table 1. Meteorites were chosen to produce a self-consistent database that includes most types of carbonaceous chondrites. Huss and Lewis (1995) collected data for Orgueil (CI), Leoville ($CV3_{red}$), Vigarano ($CV3_{red}$), Allende ($CV3_{ox}$), and Kainsaz (CO3.1). Previous work indicated that CM2 chondrites contain a very primitive assemblage of presolar grains (Amari et al., 1994; Lewis, unpublished), but high-yield chemical processing designed specifically for abundance determinations had not been done. We therefore included Murchison and Murray in our study. No CR2 chondrites had previously been studied, so we included Renazzo. In the Huss and Lewis (1995) study, reduced CV3 chondrites were represented by Leoville and Vigarano, while Allende was the only oxidized CV3 chondrite. Allende may have been meta-

Table 2. Yields of chemical processing.

Meteorite	HF-HCl residue (%)	Etched residue (%)	Diamond (ppm)	SiC + spinel (ppm)
Murchison	2.14	0.96	613	1640
Murray	2.15	0.95	560	1160
Renazzo	1.51	0.71	397	2386
Axtell	0.43	0.30	238	4530
Mokoia	1.21	0.87	430	2348
Colony	1.27	0.89	209	2669
ALHA77307	1.48	1.13	306	2790
Acfer 214	0.26	0.17	41.2	4420

Determined by direct weighing.

morphosed, so we added Axtell because previous work suggested that it is less metamorphosed than Allende (Simon et al., 1995). We also studied Mokoia, another oxidized CV3, because petrographic characteristics (McSween, 1977a) and the presence of phyllosilicates (Krot et al., 1995) indicate that it has seen lower temperatures than either Axtell or Allende. Although Huss and Lewis (1995) collected data for Kainsaz (CO3.1), it is not the most primitive CO3, and the sample used had been partly processed by other workers before the discovery of presolar grains. We therefore added ALHA77307 (CO3.0) and Colony (CO3.0) (classifications from Scott and Jones, 1990). Finally, we studied Acfer 214 (CH) to investigate how CH chondrites might be related to other carbonaceous chondrites.

2.2. Chemical Processing

Before chemical processing, samples were examined under a binocular microscope and fusion crust, weathering products, or unusual inclusions were removed. Thin sections were made for Acfer 214, Renazzo, and Axtell, and thin sections were obtained for the other meteorites for matrix abundance determination and general petrographic examination. Chemical processing was done using the high-yield procedure developed by Huss and Lewis (1995). This procedure can recover up to twice as much diamond as typical processing methods. The main tricks to this procedure are to pipette rather than decant discard liquids and to centrifuge the discard acids multiple times to assure that no solids are discarded. The chemistry itself is that developed by Lewis, Anders, and colleagues at the University of Chicago. Bulk samples were treated first with alternating cycles of 12 N HF–3 N HCl and 6 N HCl to remove silicates, followed by CS_2 to remove elemental sulfur. This HF-HCl residue was then "etched" with 0.5 N $K_2Cr_2O_7$ in 2 mol/L H_2SO_4 to remove the "normal planetary" gas component (also called P1 or Q gas) that dominates the noble gases in primitive chondrites. The resulting etched residue was then treated with $HClO_4$ at ~195°C to remove all remaining oxidizable material. Diamonds were separated by first dispersing the sample in 0.1 mol/L NH_3, which produces a diamond colloid. The sample was then centrifuged at 1000*g* for > 4 h to pull down grains > ~0.1 μm and the liquid was pipetted into a clean tube. The liquid containing the diamond was then acidified with HCl so the diamonds would flocculate together into clumps large enough to centrifuge out of the liquid. At least three cycles of colloidal separation were performed. Table 2 summarizes the results of chemical processing. A more detailed description of the chemistry can be found in Huss and Lewis (1995).

2.3. Noble-Gas Mass Spectrometry

Neon and xenon were measured for HF-HCl residues, chromic-acid-etched residues, and diamond separates for each of the eight meteorites. Samples were wrapped in platinum foil and were loaded into a glass sample tree on the sample system of the mass spectrometer. The sample system and samples were gently baked to remove adsorbed atmospheric gases. Gases were extracted by stepped pyrolysis in a tungsten coil. Samples were dropped one-at-a-time into the coil, which was heated by passing current through the coil. Temperature steps were chosen based on a current-vs.-temperature curve for the coil, and the sample temperatures were checked with an optical pyrometer. Temperatures between 800 and 1800°C should be accurate to ±25°C. Extraction times ranged from 20 min for the three low-temperatures steps to 5 min at ≥1600°C.

For each extraction step, gases were exposed for 30 min (including extraction time) to a large pellet getter containing SAES St172 getter alloy to remove the active gases. The xenon was then pulled to a charcoal finger at liquid nitrogen temperature (40 min sorption time) while the neon was exposed to a second pellet getter, a titanium flash getter, and a hot filament. Neon was then admitted to the spectrometer and measured. Residual neon in the sample system was then pumped for 5 min. The pump valve was closed and the liquid nitrogen was removed from the charcoal finger to release the xenon. The charcoal was heated to ~160°C for 25 min while the xenon was exposed to the flash getter and hot filament. Upon completion of the neon measurement, the spectrometer was pumped and xenon was admitted and measured.

Blanks were measured for various extraction temperatures before and after each sample, and calibrations of gas amount were obtained for each group of samples loaded into the spectrometer and measured. Isotopic ratios have been corrected for mass discrimination (essentially zero), isobaric interferences and blank and are reported with one-sigma measurement errors derived from counting statistics. Gas amounts are typically accurate to better than 10%. Amounts that are less precisely known are indicated.

Table 3. Compositions used to resolve Ne components.

Component	$^{20}Ne/^{22}Ne$	$^{21}Ne/^{22}Ne$
Air[a]	9.80 ± 0.08	0.0290 ± 0.0003
Ne-P1[b]	10.7 ± 0.2	0.0294 ± 0.0010
Ne-P3[c]	8.910 ± 0.057	0.029 ± 0.001
Ne-A2[d]	8.500 ± 0.057	0.036 ± 0.001
Ne-E	0	0
Solar-wind Ne[e]	13.6 ± 0.3	0.032 ± 0.004
Cosmogenic Ne #1[f]	0.825 ± 0.025	0.8875 ± 0.0375
Cosmogenic Ne #2[f]	0.79 ± 0.02	0.855 ± 0.020

[a] Eberhardt et al. (1965).
[b] Wieler et al. (1992); also known as "Q-Ne."
[c] Huss and Lewis (1994a); the low temperature component from diamonds.
[d] Huss and Lewis (1994a); pseudo-component consisting of Ne-HL + Ne-P6.
[e] Geiss et al. (1972).
[f] Cosmogenic Ne #1 is appropriate for samples dominated by chromite +spinel and was used for most residues. Cosmogenic Ne #2 is appropriate for residues dominated by spinel and was used for the etched residues of Mokoia and Axtell.

2.4. Component Resolution and Abundance Determination

The measured neon and xenon isotopic compositions were resolved into components following the methods described in Huss and Lewis (1995). The compositions of the components are given in Tables 3 and 4. Xenon compositions were resolved by mixing the components in Table 4 in various proportions until a match with the measured composition was obtained. In addition to the components in Table 4, samples also contain various amounts of radiogenic ^{129}Xe, often accompanied by excess ^{128}Xe, probably from neutron capture on iodine. For the Axtell diamond and etched residue, the sample system had a large ^{128}Xe (and ^{21}Ne) memory from previous samples irradiated for an iodine-xenon study. Therefore, acceptable matches were those in which ^{129}Xe and ^{128}Xe in the calculated compositions were less than or equal to those of the measured compositions. Abundances for the xenon components per gram of bulk meteorite were calculated by multiplying the proportions of each component by the gas content of the sample and by the fraction of the meteorite remaining as residue. Errors for the calculations consist of three parts: (1) a mixing uncertainty estimated

Table 4. Compositions used to resolve Xe components (ratios × 100).

Component	$\frac{^{124}Xe}{^{132}Xe}$	$\frac{^{126}Xe}{^{132}Xe}$	$\frac{^{128}Xe}{^{132}Xe}$	$\frac{^{129}Xe}{^{132}Xe}$	$\frac{^{130}Xe}{^{132}Xe}$	$\frac{^{131}Xe}{^{132}Xe}$	$\frac{^{134}Xe}{^{132}Xe}$	$\frac{^{136}Xe}{^{132}Xe}$
Air[a]	0.358 (2)	0.333 (2)	7.137 (21)	98.32 (35)	15.15 (5)	78.76 (25)	38.82 (11)	32.98 (8)
Xe-P1[b]	0.467 (6)	0.414 (5)	8.30 (3)	104.0 (2)	16.30 (4)	82.12 (12)	37.79 (11)	≡31.65 (10)
Xe-P3[c]	0.451 (6)	0.404 (4)	8.06 (2)	104.2 (4)	15.91 (2)	82.32 (10)	37.70 (10)	≡31.00
Xe-P6[c]	0.438 (25)	0.444 (28)	8.90 (20)	111.4 (8)	16.60 (11)	82.14 (47)	32.91 (50)	≡31.00
Xe-HL[c]	0.842 (9)	0.569 (8)	9.05 (6)	105.6 (2)	15.44 (3)	84.42 (13)	63.61 (13)	≡70.00
Xe-S[d]	0 (0.034)	0.033 (19)	21.59 (23)	11.8 (11)	48.26 (42)	18.6 (12)	2.22 (53)	≡0.34

[a] Nier (1950).
[b] Huss et al. (1996).
[c] Huss and Lewis (1994b).
[d] Lewis et al. (1994).
Uncertainties (parentheses) refer to the least-significant digits.

from the range in component abundances that produced an acceptable match combined with uncertainties for the end-member compositions, (2) the 10% uncertainty in the calibration of gas amount, and (3) the uncertainties in the total weight of the residue and in the weight of the residue fraction measured in the mass spectrometer. Different parts of the error dominate for different samples.

Neon components were deconvolved following Huss and Lewis (1995), with errors for measured compositions and uncertainties for component compositions propogated using the formalism of Rees (1984). Three neon isotopes permit unique deconvolution of only three components, but six or more neon components may be present in a given meteorite. In such cases, components must be removed or depleted through chemical processing or separated by stepped pyrolysis before component abundances can be accurately determined. The following constraints were used to limit the number of possible components. Air neon was permitted only in the first temperature step. Ne-P3, which is released from diamonds below 1000°C (Huss and Lewis, 1994a, 1994b), was permitted in etched and HF-HCl residues only for steps below 1000°C and only in samples known from diamond measurements to contain Xe-P3. Because Ne-A2 is known a priori to dominate samples that contain diamond, it was always chosen as one of the three neon components in the temperature range over which HL gases are released. These constraints allowed us to resolve the data among the components most likely to be present in the sample. As discussed in detail in Huss and Lewis (1995), calculated abundances of Ne-A2 are likely to be upper limits, and those of other components will be lower limits. To the extent that the three components chosen are the only ones present, the resulting abundances will approach the true abundances. Reported errors include the measurement errors and the uncertainties in the component abundances, the uncertainty in the abundance calibration, and the weighing uncertainties. The errors to do not include estimates of the uncertainties due to the possible presence of more than three components, but our interpretations do not depend on knowing the neon-component abundances to high precision.

3. RESULTS

The neon and xenon data are presented in Appendix 1. The abundances of the noble gas components (per gram of meteorite) used to estimate the presolar grain abundances are given in Table 5. The inferred abundances of the presolar grains in meteorites are given in Table 6 and matrix-normalized abundances are given in Table 7.

3.1. Murchison and Murray (CM2)

The neon and xenon contents of the Murchison and Murray residues are similar to those in Orgueil residues (Huss and Lewis, 1994a, 1995; Huss et al., 1996). Xenon contents of the HF-HCl residues and etched residues are within experimental uncertainties of those in Orgueil residues, while the neon contents are 10 to 15% lower. The diamond separates for Murray and Murchison appear to have 5 to 10% more xenon, but about the same amounts of neon as in the Orgueil diamonds. All three meteorites show a distinctive bi-modal release of noble gases during stepped pyrolysis (Appendix 1, Fig. 1).

The neon and xenon data from Appendix 1 have been resolved into components and are presented as ccSTP/g of bulk meteorite in Table 5. To interpret Table 5, it is necessary to understand which residues provide reliable abundance estimates and why. The HF-HCl residues, like the bulk meteorites, are dominated by the P1 noble gas component and therefore provide the best data on the amount of Xe-P1 in the sample. The abundances of Xe-P1 in the Murchison and Murray residues differ by only a few percent. Etching the HF-HCl residues with chromic acid, an oxidant, removes the P1 component and reveals the less-abundant exotic components. The etched residues are the least-processed residues that provide reliable abundance estimates of Ne-E(L), Ne-E(H), Ne-A2, Xe-HL, and Xe-S (see Huss and Lewis, 1995), and it is these results that are used to infer the abundances of the presolar carriers. The abundances of all components in the etched residues are remarkably similar for Murchison and Murray (Table 5). The inferred diamond abundances (Table 6) are higher than earlier published estimates (570 ppm in Murray, Tang and Anders, 1988; 400 ppm for Murchison, Amari et al., 1990, 1994), probably due to more-complete sample recovery in the current study. Our abundance estimate for Murchison diamonds is in good agreement with the recovered amounts from two closed-system dissolutions done at Caltech (700–800 ppm, Huss, 1997, reporting unpublished data from Chen and Huss). The inferred silicon carbide abundances are considerably higher than the amount recovered by Amari et al. (1994). They are also higher than the abundances inferred from carbon-isotope measurements (Russell, 1992). However, some of the Ne-E(H) may be carried in a phase other than silicon carbide (see below). The inferred graphite abundances are hard to compare with recovered amounts because only a portion of the graphite in graphite separates is isotopically anomalous (Amari et al., 1990, 1995). In this study, we use the gas content of a Muchison graphite separate prepared by Amari et al. (1990) to infer the graphite abundance (Table 6). The resulting abundances may be significantly different from the true amounts of presolar graphite in the meteorites. However, the error is likely to be systematic, multiplying the true abundances by a constant, so

Table 5. Abundances of tracer noble-gas components in meteorite residues (10^{-10} cc/g meteorite)[a] (see text for explanation).

Residue	^{22}Ne-E(L)	^{22}Ne-E(H)	^{22}Ne-A2[b]	^{132}Xe-P3	^{132}Xe-HL	^{132}Xe-P6	^{132}Xe-S	^{132}Xe-P1
Murchison								
HF-HCl res.	4.20 (0.42)	21.34 (2.57)	73.1 (8.5)	6.11 (1.61)	1.70 (0.35)	—	0.056 (0.043)	77.6 (7.9)
Etched res.	6.59 (0.68)	22.29 (2.25)	64.9 (7.7)	3.87 (0.41)	1.113 (0.112)	0.116 (0.026)	0.040 (0.005)	0.85 (0.11)
Diamond sep.	0.30 (0.07)[c]	1.11 (0.30)[c]	47.8 (5.2)	2.20 (0.22)	0.923 (0.094)	0.108 (0.015)	0.0036 (0.0024)	—
Murray								
HF-HCl res.	0.89 (0.21)	13.91 (1.57)	93.6 (10.4)	14.64 (2.61)	2.13 (0.32)	—	0.084 (0.048)	82.8 (8.6)
Etched res.	7.93 (0.80)	21.61 (2.21)	82.4 (8.6)	3.23 (0.35)	1.035 (0.104)	0.140 (0.036)	0.038 (0.005)	0.97 (0.14)
Diamond sep.	0.16 (0.06)[c]	0.70 (0.32)[c]	45.8 (6.5)	2.04 (0.22)	0.945 (0.099)	0.079 (0.022)	0.0053 (0.0025)	—
Renazzo								
HF-HCl res.	—	0.31 (0.09)	57.1 (5.9)	0.35 (0.25)	0.949 (0.109)	—	—	26.8 (2.7)
Etched res.	—	0.96 (0.28)	40.0 (4.1)	0.087 (0.040)	0.768 (0.079)	0.079 (0.040)	0.0028 (0.0010)	0.17 (0.05)
Diam. sep.	0.11 (0.02)[c]	0.55 (0.19)[c]	35.2 (4.6)	0.099 (0.018)	0.743 (0.084)	0.083 (0.014)	0.0018 (0.0007)	—
ALHA77307								
HF-HCl res.	—	1.0 (2.5)	34 (15)	1.35 (0.55)	0.87 (0.38)	—	—	30.7 (6.6)
Etched res.	0.11 (0.10)	4.90 (0.54)	53.2 (5.6)	0.72 (0.24)	0.818 (0.085)	0.033 (0.011)	0.0235 (0.0037)	0.31 (0.15)
Diamond sep.	—	0.17 (0.07)	26.8 (4.0)	0.361 (0.039)	0.479 (0.051)	0.062 (0.069)	0.0002 (0.0002)	—
Colony								
HF-HCl res.	—	1.14 (0.30)	20.4 (2.4)	—	0.313 (0.036)	—	0.013 (0.007)	6.66 (0.69)
Etched res.	—	1.78 (0.24)	31.9 (3.2)	0.165 (0.029)	0.514 (0.052)	0.060 (0.011)	0.0083 (0.0016)	0.37 (0.05)
Diamond sep.	0.04 (0.02)[c]	0.29 (0.12)[c]	19.7 (2.6)	0.184 (0.025)	0.352 (0.044)	0.049 (0.011)	0.0003 (0.0003)	—
Mokoia								
HF-HCl res.	—	0.006 (0.106)	56.4 (5.8)	0.379 (0.061)	0.891 (0.119)	0.048 (0.081)	0.0088 (0.0089)	15.3 (1.6)
Etched res.	—	0.32 (0.23)	59.4 (5.3)[d]	0.151 (0.026)[d]	0.892 (0.089)[d]	0.071 (0.018)	0.0010 (0.0008)[d]	0.15 (0.03)[d]
Diamond sep.	0.085 (0.030)[c]	0.64 (0.16)[c]	40.7 (4.3)	0.099 (0.012)	0.789 (0.080)	0.105 (0.013)	0.0003 (0.0005)	—
Axtell								
HF-HCl res.	—	—	27.2 (2.8)[e]	—	0.527 (0.054)[e]	—	0.0009 (0.0006)[e]	4.77 (0.48)[e]
Etched res.	0.12 (0.16)	0.030 (0.012)	30.4 (3.1)	0.003 (0.008)	0.649 (0.065)	0.055 (0.011)	0.0003 (0.0006)	0.08 (0.01)
Diamond sep.	—	0.19 (0.02)[c]	19.0 (2.8)	0.009 (0.004)	0.534 (0.063)	0.064 (0.008)	—	—
Acfer 214								
HF-HCl res.	0.038 (0.006)	0.392 (0.040)	7.36 (0.79)	0.61 (0.11)	0.114 (0.017)	0.005 (0.005)	0.0022 (0.0026)	2.64 (0.28)
Etched res.	0.179 (0.022)	0.670 (0.081)	8.6 (1.1)	0.389 (0.045)	0.144 (0.015)	0.012 (0.006)	0.0051 (0.0009)	0.29 (0.34)
Diamond sep.	0.008 (0.003)[c]	0.074 (0.018)[c]	3.60 (0.43)	0.120 (0.014)	0.069 (0.008)	0.0099 (0.0021)	0.00010 (0.00005)	—

[a] Errors (in parentheses) include counting statistics, uncertainties in the sample weight and residue weight, and 10% uncertainty in standard pipette.
[b] Pseudo-component consisting of Ne-HL and Ne-P6.
[c] Ne-E(L) and Ne-E(H) amounts in diamond separates are primarily artifacts of using a fixed composition for Ne-A2, a pseudo-component consisting of Ne-HL and Ne-P6. As the proportion of Ne-P6 increases, the composition of the mixture falls below the assumed ratio for Ne-A2, and Ne-E is calculated.
[d] Gas amounts may be 1 to 5% low due to lost 800°C step.
[e] Sample not completely outgases. Amounts may be low by 5 to 10%.

comparisons between meteorites should be valid. The Ne-E(L) contents of our residues are significantly higher than the amount of Ne-E(L) carried in the graphite separates produced by Amari et al. (1990, 1995). This difference is due primarily to larger processing losses in the previous studies, but we cannot rule out the possibility of an additional Ne-E(L) carrier.

Because the grains are sited in the matrix, the abundances must be normalized to matrix content to permit comparison between meteorites (Huss and Lewis, 1995). Matrix-normalized abundances are shown in Table 7. Using matrix abundances from McSween (1979), the matrix-normalized diamond abundances are 20 to 25% lower in CM2 chondrites than in Orgueil, the inferred silicon carbide abundances are ~50% higher, the graphite abundances are marginally lower, and the concentration of Xe-P1 is essentially the same as in Orgueil. The implications of these observations will be discussed below.

The diamond samples provide the best estimates of the relative abundances of Ne-A2, Xe-P3, Xe-HL, and Xe-P6 in the diamonds because the other noble gas components have been removed. The total gas contents and the abundances of Xe-P3, Xe-HL, and Xe-P6 are all higher in the Murchison and Murray diamonds than in Orgueil diamonds (Fig. 1). This apparently confirms the higher gas contents observed in Murray CE (Tang and Anders, 1988), which Huss and Lewis (1995) had attributed to a difference in gas calibration. Ne-A2, which dominates diamond neon, has the same abundance in Orgueil, Murchison, and Murray diamonds.

3.2. Renazzo (CR2)

The Renazzo residues have lower neon and xenon contents than the Orgueil, Murray, and Murchison residues (Appendix 1; Huss and Lewis, 1994a, 1995; Huss et al., 1996). The bi-modal gas release seen in Orgueil and the CM2 chondrites is much subdued in the HF-HCl and etched residues (Appendix 1) and is absent in the diamond sample (Fig. 1). The volatile components, Ne-E(L) and Xe-P3, are depleted by $>$ 90% in Renazzo compared to Orgueil. Matrix-normalized Ne-E(H) is depleted by ~87% and Xe-P1 is depleted by ~40% compared to Orgueil (Table 7). However, the matrix-normalized diamond abundances for Renazzo is similar to those of Orgueil and CM2 chondrites.

Table 6. Abundances of presolar components in bulk meteorites.

Meteorite	Class	Diamond[a] (ppm)	^{132}Xe-P3/^{132}Xe-HL	SiC[b] (ppm)	Graphite[c] (ppm)	^{132}Xe-P1[d] (10^{-10} cc/g)
Orgueil[e]	CI	1436 (56)	2.45 (0.07)	14.2 (0.8)	10.3 (0.4)	131.2 (3.0)
Murchison	CM2	740 (76)	2.40 (0.04)	13.5 (1.4)	4.7 (0.5)	77.7 (7.9)
Murray	CM2	614 (65)	2.18 (0.06)	13.1 (1.3)	5.6 (0.6)	82.8 (8.6)
Renazzo	CR2	410 (63)	0.133 (0.019)	0.58 (0.17)	—	26.7 (2.7)
ALHA77307	CO3.0	523 (74)	0.754 (0.013)	2.97 (0.99)	0.08 (0.07)	30.7 (6.6)
Colony	CO3.0	303 (49)	0.522 (0.026)	1.08 (0.09)	—	6.66 (0.69)
Kainsaz[e]	CO3.0	*262 (90)*[f]	0.072 (0.003)	0.055 (0.006)	—	39.5 (0.9)
Leoville[e]	CV3red	545 (18)	0.164 (0.005)	0.392 (0.013)	—	31.3 (0.8)
Vigarano[e]	CV3red	623 (20)	0.092 (0.006)	0.166 (0.012)	—	20.5 (0.5)
Mokoia	CV3ox	484 (69)	0.125 (0.009)	0.19 (0.14)	—	15.3 (1.6)
Axtell	CV3ox	289 (19)	0.017 (0.007)	0.018 (0.009)	0.09 (0.11)	4.77 (0.48)[g]
Allende[e]	CV3ox	340 (45)	0.012 (0.007)	0.0062 (0.0049)	—	11.5 (0.9)[h]
Acfer 214	CH	86.6 (9.9)	1.75 (0.03)	0.41 (0.05)	0.13 (0.02)	2.64 (0.28)

[a] Calculated using Xe-HL content of diamond sample and Xe-HL in etched residue.
[b] Assuming a Ne-E(H) content for SiC of $16{,}500 \times 10^{-8}$ ccSTP/g, see Huss and Lewis (1995).
[c] Assuming a Ne-E(L) content for graphite of $14{,}000 \times 10^{-8}$ ccSTP/g (Amari et al., 1990).
[d] Abundance calculated from the HF-HCl residue.
[e] Data from Huss and Lewis (1994b, 1995) and Huss et al. (1996).
[f] Sample subject to excessive processing losses, see Huss and Lewis (1995).
[g] Axtell HF/HCl residue was not fully out-gassed. Amount of Xe-P1 may be 5 to 10% low.
[h] Calculated from residues 3C1 and 3CS1 from Lewis et al. (1975).

3.3. CO3 Chondrites

The ALHA77307 (CO3.0) and Colony (CO3.0) residues have much lower neon and xenon contents than Orgueil and CM2 residues and somewhat lower gas contents than Renazzo residues (Appendix 1; Huss and Lewis, 1994a, 1995; Huss et al., 1996). The HF-HCl residues have less gas than the HF-HCl residues from Kainsaz (CO3.1) measured by Alaerts et al. (1979) and Huss et al. (1996). The matrix-normalized Xe-P1 content for Kainsaz is indistinguishable from that for Orgueil (Table 7), while ALHA77307 and Colony have ~85 and ~18%, respectively, of the Xe-P1 in Kainsaz. The low gas content for the Colony HF-HCl residue may be due in part to

Table 7. Matrix-normalized abundances of presolar components for carbonaceous chondrites along with ^{132}Xe-P3 and ^{132}Xe-P6 abundances in their diamond.

Meteorite	(Matrix fraction)	Class	Diamond (ppm)	SiC (ppm)	Graphite (ppm)	^{132}Xe-P1 (10^{-10} cc/g met.)	^{132}Xe-P3 in diamond (10^{-10} cc/g)	^{132}Xe-P6 in diamond (10^{-10} cc/g)
Orgueil	(1.00)	C1	1436 (63)[a]	14.2 (0.8)[a]	10.3 (0.4)[a]	131.2 (2.7)[a]	3442 (96)[a]	131 (8)[a]
Murchison	(0.636)[b]	CM2	1164 (119)	21.2 (2.2)	7.4 (0.8)	122.2 (12.4)	3606 (364)	177 (26)
	(0.515)[c]		*1437 (148)*	*26.2 (2.7)*	*9.1 (1.0)*	*150.9 (15.3)*		
Murray	(0.588)[b]	CM2	1044 (111)	22.3 (2.2)	9.5 (1.0)	140.8 (14.6)	3681 (394) [4120 (220)[d]]	142 (40) [175 (18)[d]]
	(0.428)[c]		*1435 (152)*	*30.6 (3.0)*	*13.1 (1.4)*	*193.5 (20.1)*		
Renazzo	(0.311)[e]	CR2	1318 (203)	1.86 (0.55)	—	85.9 (8.7)	250 (45)	208 (36)
ALHA77307	(0.337)[f]	CO3.0	1551 (220)	8.8 (1.6)	0.08 (0.07)	91 (20)	1180 (203)	205 (35)
Colony	(0.293)[g]	CO3.0	1034 (167)	3.69 (0.31)	—	22.7 (2.4)	887 (121)	235 (53)
Kainsaz	(0.300)[h]	CO3.1	873 (304)[a]	0.183 (0.022)[a]	—	131.5 (2.8)[a]	139 (7)[a]	260 (10)[a]
Leoville	(0.351)[e]	CV3red	1554 (93)[a]	1.12 (0.07)[a]	—	89.1 (2.1)[a]	317 (12)[a]	267 (11)[a]
Vigarano	(0.345)[e]	CV3red	1806 (107)[a]	0.481 (0.042)[a]	—	59.5 (1.4)[a]	156 (10)[a]	191 (11)[a]
Mokoia	(0.398)[e]	CV3ox	1216 (173)	0.48 (0.35)	—	38.4 (4.0)	230 (29)	245 (30)
Axtell	(0.35)[f]	CV3ox	826 (83)	0.051 (0.026)	0.25 (0.31)	13.6 (1.3)	38 (16)	270 (35)
Allende	(0.384)[e]	CV3ox	885 (125)[a]	0.016 (0.013)[a]	—	30 (5)[i]	27 (15)[a]	269 (16)[a]
Acfer 214	(0.12)[fj]	CH	721 (110)	3.41 (0.54)	1.08 (0.20)	22.0 (3.2)	2915 (332)	241 (52)

[a] From Huss and Lewis (1994b, 1995). Errors (in parentheses) include the 2% uncertainty in the gas amount.
[b] Matrix abundance from McSween (1979).
[c] Matrix abundance modified to bring diamond abundance into line with Orgueil.
[d] Data for Murray CE as calculated by Huss and Lewis (1994b).
[e] Matrix abundance from McSween (1977a).
[f] Matrix abundance from this study.
[g] Matrix abundance from Rubin et al. (1985).
[h] Matrix abundance from McSween (1977b).
[i] Calculated from residues 3C1 and 3CS1 from Lewis et al. (1975).
[j] Dark inclusions (3% of meteorite) are not included in matrix abundance.

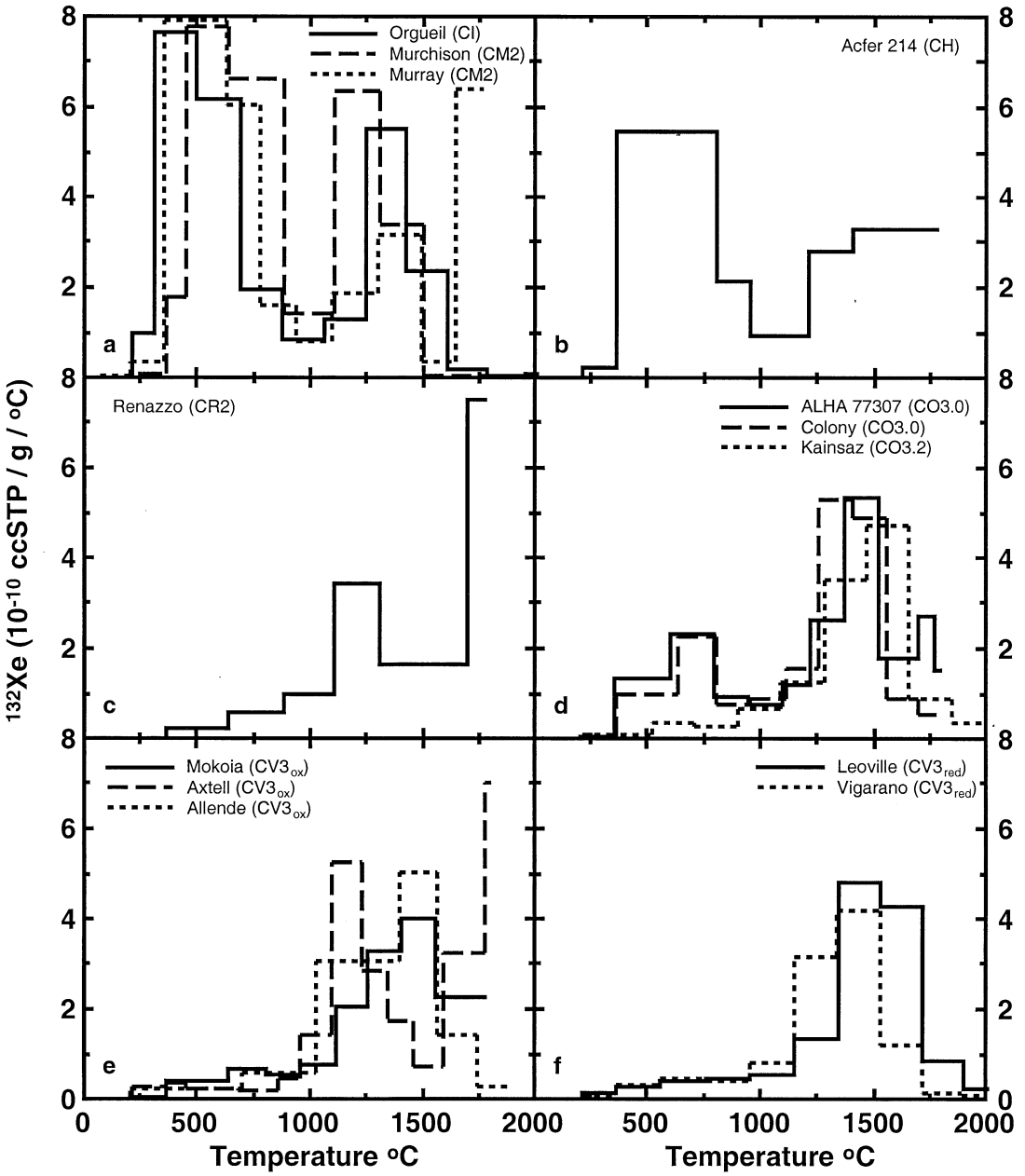

Fig. 1. Xenon release patterns for the diamond fractions from the carbonaceous chondrites studied here. The temperature steps are normalized to °C so that the areas under the curves accurately represent the gas amounts. Note the distinct bi-modal release pattern for CI and CM2 chondrites (top left) and for Acfer 214 (top right). The low-temperature release is the P3 component, which has approximately "normal" isotopic composition (Huss and Lewis, 1994a). The high-temperature release is dominated by the isotopically anomalous HL component. Most samples show some degree of depletion of the low-temperature gas.

unrepresentative sampling. The Colony residue was very sticky and hard to work with before chromic-acid etching, forming tar balls that could not be easily sampled. The abundances of Ne-A2 and Xe-HL normalized to bulk meteorite are ~40% lower in the HF-HCl residue than in the etched residue (Table 5). However, the Ne-A2/Xe-HL ratio is the same in both residues. A residue cannot gain gas or presolar components from chemical processing, so we conclude that our supposed aliquot of the HF-HCl residue from Colony was actually a fractionated sample dominated by gas-free phases. Thus, the abundance of Xe-P1 for Colony is probably too low by ~40%. The low Xe-P1 abundance inferred for Colony may also reflect terrestrial weathering. Colony is a heavily weathered find from Oklahoma, while Kainsaz is a witnessed fall. Similar low Xe-P1 abundances compared to witness falls have been noted previously for Ragland, a weathered LL3.5 chondrite from New Mexico (Huss et al., 1996) and for RC075, a weathered H3.2 chondrite from New Mexico (McCoy et al., 1993). For

Table 8. Summary of the history of the most primitive members of each carbonaceous chondrite group.

Class	Chondrules	Metal/silicate fractionation	Temp. (°C)[a] of high-*T* component	Low-*T* component present	Temp. (°C) of low-*T* component	% chond.[b]	% matrix	% low-*T* comp. in matrix	Parent body temp. (°C)[c]
CI	No	None	—	Yes	Cold		~100	95–100	≤150
CM2	Yes	None	~400	Yes	Cold	~50	~50	95–100	≤100
CO3	Yes	~None	~400	Yes	<200–250	~70	~30	40–70	≤200
CR2	Yes	~None	400–450	Minor	Cold	~70	~30	~5	~150
CH	Yes	Major	400–450	Inclusions	Cold	85	12	3% of met.	≤150
CV3	Yes	Moderate	550–600	Yes	≤300	60–65	35–40	5–10	≤300

[a] Temperatures listed here are based on abundances of presolar components in meteorites and may be too low. Bulk compositional data and experiments on the stability of silicon carbide may require upward revisions of ~300°C (see text).
[b] In this context, "chondrules" means chondrules, CAIs, metal, troilite, large anhydrous mineral grains, etc.
[c] This temperature is that indicated for the least metamorphosed member of the group. Other meteorites experienced higher metamorphic temperatures.

these reasons, we will largely ignore the Xe-P1 abundance inferred for Colony in the following discussions.

The gas contents of the ALHA77307 and Colony etched residues are similar to that of the Kainsaz etched residue prepared by Alaerts et al. (1979). About 60 to 70% of the diamonds inferred to be present from the etched residues were recovered in the ALHA77307 and Colony diamond separates. The calculated Ne-E(L) and Ne-E(H) abundances are much lower in CO3s than in CI and CM2 chondrites. A trace of Ne-E(L) was detected in the ALHA77307 etched residue (Tables 5), but Ne-E(L) was not resolved for Colony. Ne-E(H) was resolved for the etched residues of both ALHA77307 and Colony. The Ne-E(L) and Ne-E(H) abundances in Table 5 are probably lower limits due to residual solar Ne and Ne-P1. Huss and Lewis (1995) showed that higher and more reliable abundances for Ne-E(H) in CO and CV chondrites can be obtained from the more-highly-oxidized SiC + spinel separates because Ne-P1 and other components are more completely removed. However, even the lower limits on Ne-E(H) given in Table 5, when normalized to matrix content, are 62 and 26% for ALHA77307 and Colony, respectively, of the matrix-normalized Ne-E(H) amount for Orgueil (Table 7). The Ne-E(H) number for Kainsaz matrix (~1% of the amount in Orgueil) was determined from the SiC + spinel separate (Huss and Lewis, 1995) and is likely to be close to the true value.

Diamonds from both ALHA77307 and Colony exhibit a bimodal release of noble gases, although the low-temperature P3 peak is not as large as in CI and CM2 chondrites (Fig. 1). The releases of the Xe-P3 in these two diamond samples is offset to slightly higher temperatures, implying that this gas is the residual of an original component like that in CI and CM2 diamonds. This behavior was also seen in LL3.0 to LL3.1 chondrites (Huss and Lewis, 1994a, 1994b). The matrix-normalized diamond abundance in Colony is similar to that in CM2 chondrites, while the lower limit on the silicon carbide abundance is ~25% of that in Orgueil (Table 7).

3.4. Mokoia and Axtell ($CV3_{ox}$)

Neon and xenon contents of the Mokoia and Axtell residues are lower than in CI and CM2 residues. There is very little low-temperature gas in any of the residues (Appendix 1, Fig. 1). The 800°C fraction for the Mokoia etched residue was accidentally pumped away to the ion gauge, but gas releases for the HF-HCl residue and diamond separate indicate that no more than 2% of the neon and 5% of the xenon were lost. The 800°C step was important for Ne-E(L), but the high abundance of solar neon in the Mokoia etched residue would have precluded a reliable Ne-E(L) estimate from that step in any case. The upper limit on the amount of Ne-E(L) in Mokoia, using very favorable assumptions, is < 4% of that in CI and CM2 chondrites. A similar upper limit was inferred for Axtell, although Ne-E(L) was not resolved in any low-temperature step.

Estimates of diamond and silicon carbide abundances in Mokoia are not affected by the loss of the 800°C step because their tracer gases are not released at this temperature. Mokoia has ~50% more diamond in its matrix than do Axtell and Allende, but the Mokoia abundance is not as high as that for Orgueil (Table 7). The Xe-P3/Xe-HL ratio in diamonds is nearly ten times higher in Mokoia than in Axtell. The abundances for silicon carbide have large uncertainties. For Mokoia, Ne-E(H) is marginally resolved in the 1300, 1450, and 1610°C steps, in spite of the presence of solar neon and Ne-P1. Because solar neon and Ne-P1 mask Ne-E(H) in the calculations, the silicon carbide abundance in Table 7 is a lower limit (cf. Huss and Lewis, 1995). For Axtell, which has much less solar neon, the deconvolution calculations show marginal evidence for Ne-E(H) in the 1225 and 1400°C steps. This again is probably a lower limit, but the low calculated Ne-P1 abundance indicates that it is close to the correct amount.

3.5. Acfer 214 (CH)

Neon and xenon contents of the Acfer 214 residues are lower than those of CM2 residues and similar to residues of CR2, CO3, and CV3 chondrites (Appendix 1). Acfer 214 diamonds show a clear bimodal gas release (Fig. 1). The Xe-P3/Xe-HL ratio is ~75% of that in CM2 diamonds, much higher than in CR2, CO3, and CV3 diamonds (Table 7). Acfer 214 shows clear evidence of Ne-E(L) and its graphite carrier, but the inferred abundance is ~10% of that in CI and CM2 chondrites (Table 8). The matrix-normalized diamond abundance is ~50% of that in CM2 chondrites and Orgueil, and the silicon carbide abundance is ~24% of that in Orgueil (Table 7).

4. DISCUSSION

The abundances and characteristics of presolar grains can be combined with bulk compositional information for the host meteorites to infer relationships among chondrite groups and to infer something about the nebular processing that produced those groups. In the discussion below, we will first attempt to establish the characteristics of the most primitive (least fractionated) material in chondritic meteorites. Then we will show that the abundances and characteristics of presolar grains and the bulk compositional properties of the host meteorite correlate in the other classes of carbonaceous chondrites. We will argue that the same nebular processing produced both sets of properties. If our analysis is correct, it implies that the dominant processes that produced the chondrite groups were fractional evaporation of the complex of presolar dust inherited from the sun's parent molecular cloud and mixing of components that had experienced different levels of evaporation. Nebular condensation is relegated to a secondary role. The metal-silicate fractionation that is so important in the development of ordinary and enstatite chondrites (e.g., Larimer and Anders, 1970) does not play an important role in the histories of most carbonaceous chondrites.

4.1. Primitive Material

4.1.1. CI Chondrites

The chondrites with bulk compositions closest to that of the solar chromosphere are the CI chondrites (e.g., Anders and Grevesse, 1989). This compositional similarity suggests that CI chondrites accreted an approximately representative sample of the solid elements in the Sun's parent molecular cloud. The Orgueil CI chondrite has high abundances of presolar diamond, silicon carbide, and graphite (Tables 6 and 7), and its diamonds have among the highest concentrations of low-temperature P3 gases (Huss and Lewis, 1995). The tables also show the abundance of Xe-P1, the major noble gas component in chondrites. Although the carrier for Xe-P1 is not known, there are good reasons to believe that it too is presolar (Huss and Alexander, 1987; Huss et al., 1996). Orgueil contains presolar oxides (Hutcheon et al., 1994). It also contains anomalous chromium (e.g., Podosek et al., 1997) and s-process molybdenum (Dauphas et al., 2002) not seen in more processed chondrites. Finally, Orgueil contains deuterium-enriched organic matter (bulk $\delta D \approx +1360‰$; e.g., Robert and Epstein, 1982; Halbout et al., 1990) that is thought to reflect low-temperature ion-molecule reactions in the Sun's parent molecular cloud (e.g., Kerridge, 1983). The known presolar materials in Orgueil thus span the range of thermal resistance and include both oxidized and reduced types. The bulk compositional data and data for presolar components suggest that CI chondrites sampled the bulk reservoir of presolar material in the Sun's parent molecular cloud. The major mineralogy of CI chondrites is no longer that of molecular cloud material, however. Aqueous activity on the meteorite parent body has almost completely transformed the mineralogy of these meteorites. Orgueil has less-anomalous hydrogen in its organic matter than do lightly altered meteorites like Renazzo (CR2) and Bishunpur (LL3.1) (e.g., Yang and Epstein, 1983), probably because the aqueous alteration also affected the anomalous organics. However, presolar diamond, silicon carbide, and graphite survive extensive acid treatments in the laboratory and thus were probably not affected by aqueous alteration on the meteorite parent body.

4.1.2. CM2 Chondrites

The CM2 chondrites consist of 50 to 60% fine-grained hydrated matrix material and 40 to 50% chondrules and CAIs (McSween, 1979). The bulk composition of the matrix material is very similar to that of CI chondrites. Figure 2 shows the bulk compositions of Murchison and Murray normalized to CI chondrites with the elements arranged in order of decreasing volatility. The elements more volatile than potassium are depleted by ~40%, those from gold through nickel are enriched by ~14%, and elements more refractory than uranium are enriched by ~32% relative to CI chondrites. This pattern is broadly consistent with a two-component model in which CM2 chondrites are composed of ~50% matrix material with a CI-like composition and ~50% material largely depleted in volatile elements, such as chondrules, CAIs, and metal (e.g., Wolf et al., 1980). The high-temperature component consists of two parts. CM2 chondrites contain a few percent CAIs (McSween, 1979), many of which are enriched in refractory trace elements by factors of ~10 to 100 (e.g., Ireland, 1990). A high-*T* component with ~10% CAIs (~5% of the bulk meteorite) would show the observed extra enrichments of the most refractory elements over iron and magnesium, which are major constituents of chondrules but are depleted in CAIs.

CM2 chondrites contain high abundances of diamond, silicon carbide, graphite, and the Xe-P1 carrier (Tables 6 and 7). They also contain deuterium-rich organic matter (bulk $\delta D = +1000$ to $+1200‰$) (e.g., Kerridge, 1983; Yang and Epstein, 1983). To first order, the abundances of known types of presolar material, both labile and thermally resistant, are similar to those in Orgueil (CI) (Fig. 3). There are some second-order differences, but some of these may be artifacts of the abundance calculations. For example, the matrix-normalized diamond abundances for Murchison and Murray are 20 to 25% lower than that for Orgueil, and the graphite abundances are also somewhat lower (Table 7). But the Xe-P3/Xe-HL ratios for diamonds from Murchison and Murray (Table 6) are similar to ratios determined previously (2.00–2.37, Lewis, unpublished; 2.53, Tang and Anders, 1988, respectively) and to that for Orgueil diamonds (2.46; Huss and Lewis, 1995). The high Xe-P3/Xe-HL ratios would seem to preclude thermal destruction as a reason for the lower diamond and graphite abundances. One possibility is that the estimates of matrix fraction used to normalize the abundances (from McSween, 1979) are not appropriate. For example, Grossman and Olsen (1974) estimated the Murchison matrix content to be ~50%, compared to ~63.6% by McSween (1979). Petrographic matrix in CM2 chondrites may not correspond directly to the fine-grained nebular dust component due to extensive aqueous alteration. McSween (1979) showed that the matrix fraction correlates with the degree of alteration in CM2 chondrites and postulated that anhydrous minerals have been converted into fine-grained phyllosilicates (petrographic matrix). Matrix abundances of 51.5 and 42.8% for Murchison and Murray, respectively, bring

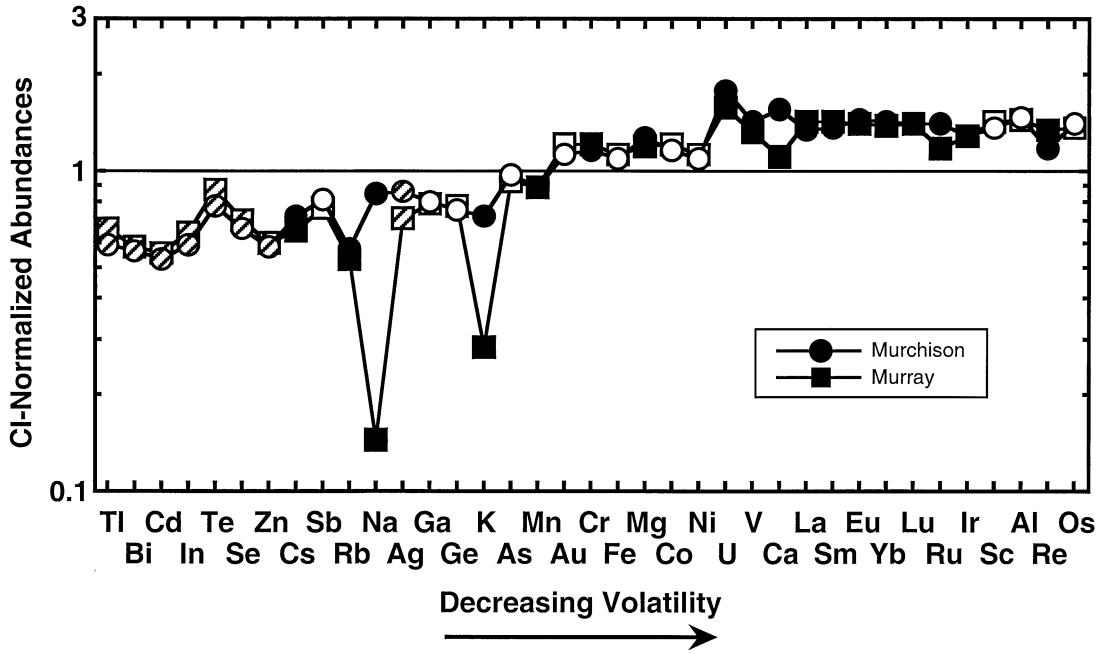

Fig. 2. Abundances of 37 elements in the Murchison and Murray CM2 chondrites normalized to the abundances in CI chondrites. The elements are arranged in order of decreasing volatility from left to right. Siderophile elements are shown with open symbols, chalcophile with partially filled symbols, and lithophile elements with solid symbols. Elements more volatile than potassium are systematically depleted by ~40%, gold to nickel are enriched by ~14%, and elements more refractory than uranium are enriched by ~32% compared to CI chondrites. This pattern is consistent with a two-component mixture of CI-like matrix and thermally processed chondrules, CAIs, metal, etc. (see text). Low sodium and potassium for Murray are attributed to leaching after the fall (Kallemeyn and Wasson, 1981). Data for Murchison and Murray are from Kallemeyn and Wasson (1981) and Krähenbühl et al. (1973). Abundances for CI chondrites are from Anders and Grevesse (1989).

the diamond abundances into line with that of Orgueil, and the graphite abundances bracket the Orgueil abundance. This calculation results in somewhat higher Xe-P1 abundances for Murchison and Murray than in Orgueil, and the already high inferred silicon carbide abundances are even higher (Fig. 3). However, the inferred silicon carbide abundances for Murchison and Murray may not be correct.

4.1.3. Another Ne-E(H) Carrier?

The high inferred silicon carbide abundances for Murchison and Murray (Table 7) are based on Ne-E released above ~1100°C and are not supported by either the mass of recovered separates generated by Amari et al. (1994) or by estimates from carbon isotopes in meteorite residues (Russell, 1992). The high Ne-E(H) abundances may reflect the presence of another Ne-E(H) carrier. There have been previous hints of another Ne-E(H) carrier. The HF-HCl residue from Orgueil processed by Huss and Lewis (1995) contained ~70% more Ne-E(H) than did the etched residue. The Murchison and Murray residues do not show a difference between HF-HCl and etched residues (Table 7), but the amount of Ne-E(H) is about twice that in the Orgueil etched residue. If CI and CM2 data both reflect a second Ne-E(H) carrier, it is not clear why the carrier survived etching in CM2 chondrites and not in Orgueil. Perhaps there was a slight difference in etching temperature or duration between the two studies, or perhaps the history of the meteorites changed the sensitivity of the carrier to oxidation. In any case, the evidence would seem to suggest that a Ne-E carrier that is thermally resistant but moderately susceptible to oxidation is present in CI and CM2 chondrites. Our best estimate of the matrix-normalized silicon carbide abundance in CI and CM2 chondrites is ~14 ppm, which implies that ~30 to 50% of the Ne-E(H) in these meteorites is located in this other carrier. This material may also be a carrier of the s-process molybdenum described by Dauphas et al. (2002).

4.1.4. Properties of Primitive Nebular Material

CI chondrites and CM2 matrices have essentially unfractionated bulk chemical compositions. They contain roughly the same high abundances of presolar diamonds (~1400 ppm), their diamonds have the highest Xe-P3/Xe-HL ratios (~2.4), both classes have high abundances of Ne-E(L) and, presumably, of presolar graphite (~10 ppm, matrix normalized), both classes have high abundances of silicon carbide and both appear to have a second, less resistant carrier of Ne-E(H), and both classes have high abundances of Xe-P1. Thus, both CI chondrites and CM2 matrix contain high abundances of thermally labile and thermally resistant, chemically reactive and chemically resistant materials, and neither the bulk compositions nor the assemblages of presolar grains appear to have been fractionated. This implies that these materials were never exposed to high temperature, either in the nebula or on the meteorite parent body. CI and CM2 chondrites experienced extensive aqueous alteration. This may reflect a low accretion

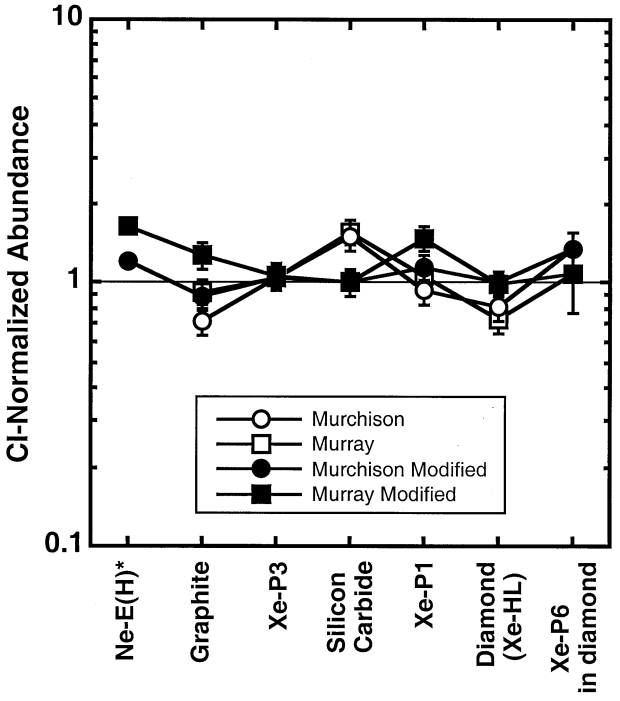

Fig. 3. Abundances of presolar components in CM2 chondrites normalized to the abundances in Orgueil. The components are arranged in order of increasing resistance to chemical and thermal destruction from left to right. These components have been normalized to the matrix abundances in CM2 chondrites, except for Xe-P3 and XeP6, which are abundances in the diamond separates. Open symbols show normalized abundances assuming matrix contents from McSween (1979). Filled symbols show abundances using matrix contents that make diamond abundances equal to that of Orgueil and which assign excess Ne-E(H), defined as Ne-E(H)*, to a separate, less resistant carrier (see text). Orgueil abundances are from Huss and Lewis (1995).

temperature, which permitted water ice to accrete into the meteorite parent bodies. For the purposes of the following discussion, we will consider the CI chondrites and CM2 matrix to be most representative of the raw material for the solar system, both in terms of bulk composition and in terms of the mixture of presolar components. For simplicity and because the characteristics of CI chondrites are better constrained, we will normalize the bulk compositional data and the presolar-grains data to CI chondrites. Minor differences between CI chondrites and CM2 matrices do not affect our conclusions.

4.2. Processed Material and Mixtures

4.2.1. CR2 Chondrites

Figure 4 compares the bulk compositions for Renazzo and average CR2 chondrites and abundances of presolar components for Renazzo to those of Orgueil. Both panels are arranged in order of decreasing volatility/chemical-thermal resistance from left to right. To first order, the characteristics of CR2 chondrites reflect simple temperature-driven fractionation in which volatile elements were lost and the most fragile presolar components were destroyed. The bulk compositions have flat patterns for elements more refractory than chromium, with the refractory elements uniformly enriched relative to CI by 40 to 43% (Fig. 4a). Elements more volatile than chromium are depleted relative to the refractory element "plateau," with the degree of depletion increasing with increasing volatility. There is no step in the refractory elements comparable to that seen in CM2 chondrites, which reflects the low abundance of CAIs in CR2 chondrites (~0.3% in Renazzo; McSween, 1977a). A mass-balance calculation including all volatile elements shows that the enrichments of refractory elements are a direct result of the loss of volatiles. There is no evidence of metal-silicate fractionation in CR2 chondrites.

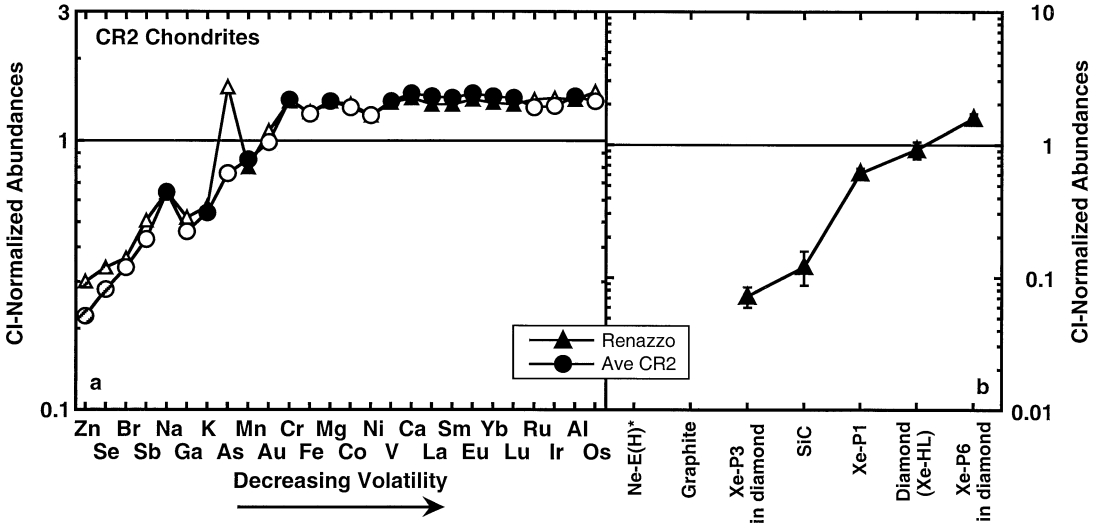

Fig. 4. Data for bulk compositions and presolar components, normalized to CI chondrites, are shown for Renazzo and average CR2 chondrites. Plotting conventions are the same as in Figures 2 and 3. Elements more refractory than chromium show a flat pattern at 40 to 43% enrichment relative to CI, while volatile elements show increasing depletions with increasing volatility. The arsenic number for Renazzo appears to be in error. All presolar components are depleted relative to CI except Xe-P6, which is enriched by ~60%. Depletions are greatest for the least resistant components. Bulk compositional data for CR2 chondrites from Kallemeyn and Wasson (1982) and Kallemeyn et al. (1994).

The most volatile elements are more severely depleted in CR2 than in CM2 chondrites, in part reflecting a lower percentage of matrix, but also indicating that the matrix is depleted in the most-volatile elements. The elemental fractionation patterns reflect the entire meteorite. Thus, losses of volatiles during production of chondrules and CAIs are reflected in the bulk composition. Volatile loss during chondrule formation may not be complete due to the short time scale (e.g., Yu et al., 1996). Connolly et al. (2001) argue that CR2 chondrule precursors were already depleted in volatile elements such as gold before chondrule formation. CR2 metal grains that apparently formed by recondensation of siderophile elements evaporated from chondrules are depleted in gold relative to CI chondrites. Such condensates would be enriched in gold and other volatile siderophiles relative to CI chondrites if they condensted from material produced by incomplete evaporation from a CI composition. Thus, elements with volatility similar to or greater than gold were probably depleted relative to CI in the CR formation region before production of chondrules. Although there is good chemical evidence for temperature-driven fractionation in the CR formation region, the chemical data probably do not provide numerical constraints on temperature, primarily because the bulk compositions have also been affected by chondrule formation.

In contrast to the bulk compositions, the presolar components reflect only the matrix. Abundances of these components also decrease with decreasing thermal and chemical resistance (Fig. 4b), with only Xe-P6, the most refractory component of presolar diamond (Huss and Lewis, 1994a, 1994b), enriched relative to CI. Presolar components provide several essentially independent ways to investigate the thermal history of a meteorite. The P3 noble-gas contents give the maximum temperature experienced by presolar diamonds, either before or after accretion, and the release of P3 gases seems to be essentially independent of the nature of the surroundings (Huss and Lewis, 1994b). The Xe-P3 content of Renazzo diamonds is similar to that of diamonds from Bishunpur (LL3.1), which experienced a metamorphic temperature of ~300°C (cf. Huss and Lewis, 1994b). The heating recorded by Renazzo diamonds destroyed most of the P3 carrier and some of the HL carrier, producing a ~60% enrichment of Xe-P6 in the surviving diamonds.

Other presolar components provide less quantitative estimates of temperature. The silicon carbide abundance for Renazzo is considerably lower than that for Bishunpur and slightly lower than that for Krymka (LL3.1) (cf. Huss and Lewis, 1995); graphite (Ne-E[L]) was not detected in Renazzo. Among ordinary chondrites, a 90% depletion of silicon carbide and an absence of graphite would imply a type 3.5 meteorite (Huss and Lewis, 1995), for which metamorphic temperatures of 400–500°C have been estimated (Huss and Lewis, 1994b). This temperature is consistent with the presence of organic matter in Renazzo matrix with a much higher bulk δD (~+2200‰) than that in CI and CM2 chondrites (Yang and Epstein, 1983). The deuterium-rich hydrogen is released by pyrolysis at 500°C and above, but is not released at 350°C (Yang and Epstein, 1983). Thus, the organic carriers could not have experienced a temperature approaching 500°C during their history or they would have been destroyed. The silicon carbide and graphite abundances and the deuterium-rich organic compounds imply a processing temperature of 400 to 450°C. However, this temperature appears to be inconsistent with the ~300°C recorded by P3 gases in the diamonds, which suggests that a small amount of P3-rich diamonds was added after the peak processing temperature.

The 400 to 450°C estimated processing temperature for the bulk of the presolar dust probably does not reflect metamorphism in the host meteorite. Renazzo has experienced aqueous alteration that affected chondrule mesostasis, dark inclusions, and matrix (Weisberg et al., 1993). This alteration is less severe than that in CI and CM2 chondrites, however, and it did not affect the deuterium-enriched organic materials inherited from the presolar molecular cloud (Yang and Epstein, 1983), as it appears to have done in CI and CM2 chondrites. The phyllosilicate assemblage and the absence of tochilinite in CR2 chondrites imply a maximum temperature of ~150°C for aqueous alteration (Zolensky, 1991). Temperature estimates based on oxygen-isotope data appear discordant, with the carbonate-phyllosilicate thermometer indicating a temperature of $<$ 150°C and the phyllosilicate-magnetite thermometer indicating a temperature of ~300°C (Weisberg et al., 1993). The metamorphic temperature experienced by the meteorite as a whole is the lowest maximum temperature experienced by any of its components. Thus, the above data imply that the Renazzo meteorite experienced a metamorphic temperature of ~150°C, and that the 400 to 450°C processing recorded by the presolar grains occurred before accretion.

The combined chemical and presolar-grains data indicate that the main reservoir of CR precursors experienced temperatures of 400 to 450°C during the nebular processing that defined the CR bulk composition. Chondrules, metal, and other high-temperature components in CR2 chondrites formed from this reservoir, but the matrix did not experience the chondrule-forming event. The region cooled and the CR2 chondrites accreted. During accretion a small amount of volatile-rich material was added, providing some P3-rich diamonds and perhaps providing the water for aqueous alteration. After accretion, matrix and chondrules experienced parent-body temperatures of ~150°C during aqueous alteration and metamorphism.

4.2.2. CO3 Chondrites

Normalized bulk compositions of CO3 chondrites are shown in Figure 5a. The CO3 patterns show clear evidence of volatility control, but they are more complicated than those of CR2 chondrites (cf. Figs. 4a and 5a). Colony, Kainsaz, and average CO3 chondrites are indistinguishable from one another and show uniform enrichments (60–65%) of the most refractory elements (vanadium to osmium) compared to CI chondrites. Elements from gold to nickel are enriched by 30 to 35%, and the more volatile elements show generally increasing depletions with increasing volatility. ALHA77307 has a similar enrichment pattern for the refractory and intermediate elements, but the enrichments are somewhat lower, leading some to question whether ALHA77307 should be classified as a CO3 (e.g., Kallemeyn and Wasson, 1982). But the difference seems best explained by a higher matrix content of ALHA77307 (~43%, Scott et al., 1981) compared to the CO3 chondrites plotted in Figure 5 (~30–33%, McSween, 1977b; Rubin et al., 1985). The step in the abundances of refractory elements at

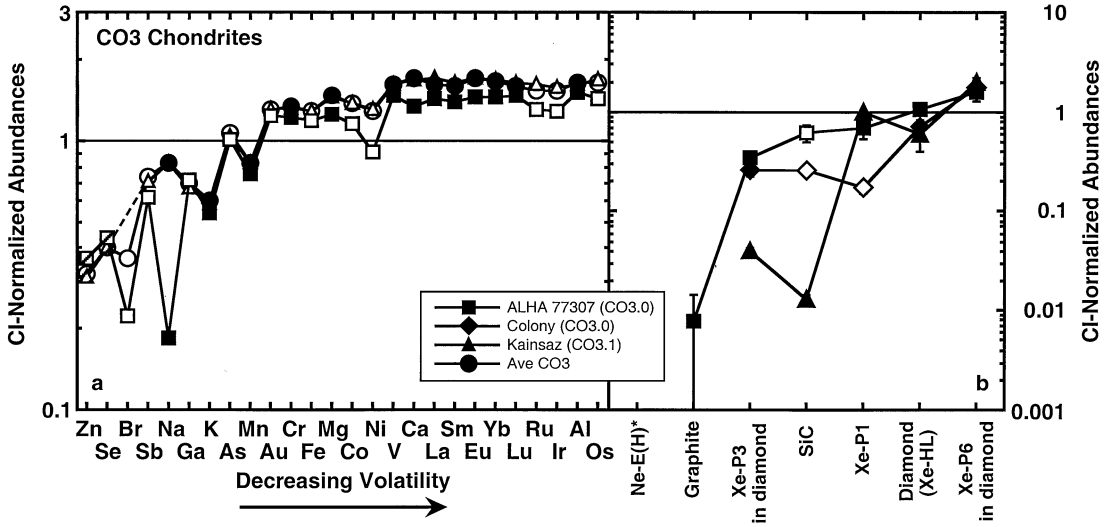

Fig. 5. Bulk compositional data for ALHA77307, Kainsaz, and average CO3 chondrites and abundances of presolar components for ALHA77307, Colony, and Kainsaz are shown. Plotting conventions follow previous Figures. (a) The bulk compositions can be divided into three regions: refractory elements from vanadium to osmium, elements of intermediate volatility from gold to nickel, and volatile elements, which show generally increasing depletions relative to CI chondrites with increasing volatility. ALHA77307 shows smaller enrichments of refractory and intermediate elements than do other CO3 chondrites. Extreme depletions of bromine and sodium in ALHA77307 are probably due to weathering (Kallemeyn and Wasson, 1982). (b) Abundances of presolar components generally correlate with chemical and thermal resistance. ALHA77307 shows the least fractionated presolar-grain pattern. The SiC abundance for ALHA77307 and Colony (open squares) are probably lower limits on the true abundances (see text). The Xe-P1 abundance for Colony (open diamond) is probably low due to unrepresentative samples and terrestrial weathering (see text). Note that the matrix content measured in our sample of ALHA77307 (~33.7%; Table 7) was used to normalize the abundances for ALHA77307. Bulk compositional data are from Kallemeyn and Wasson (1981, 1982). Abundance data for Kainsaz are from Huss and Lewis (1994a, 1994b, 1995).

vanadium probably reflects the presence of ~2% CAIs (McSween, 1977b), which are enriched to ~20 to 100 × CI in the most-refractory elements (e.g., Russell et al., 1998). There is little evidence of metal/silicate fractionation, except in ALHA77307, where siderophiles are slightly depleted.

The bulk compositions indicate that the CO3 chondrite precursors were not heated as much as the CR2 precursors before accretion. Unlike in CR2 chondrites, gold is not depleted relative to chromium, iron, and magnesium. Depletions of the most volatile elements are marginally less extreme than in CR2 chondrites, even though the matrix abundances are similar in CO3 and CR2 chondrites. In addition, the enrichment levels of the refractory elements not concentrated in CAIs (gold through nickel) are slightly less than in the CR2 chondrites.

Abundance patterns of presolar components show the effects of several different processes (Fig. 5b). ALHA77307 (CO3.0) shows the shallowest pattern compared to CI, which indicates that its matrix has seen the lowest temperature of the meteorites studied. The high Xe-P3 content of ALHA77307 diamonds supports this conclusion (Fig. 1, Table 7). Colony (CO3.0) has a steeper pattern, and Kainsaz (CO3.1) shows the largest depletions of diamond, silicon carbide and Xe-P3 in its diamonds. However, Kainsaz has the highest Xe-P1 content. Neither Colony nor Kainsaz shows any evidence for graphite, and none of the CO3s shows evidence for the chemically reactive Ne-E(H)* carrier. Diamonds from all three meteorites show enrichments of Xe-P6, with Kainsaz showing the greatest enrichment (Table 7).

The steeper abundance patterns for Colony and Kainsaz relative to that for ALHA77307 probably reflect differences in the level of parent body metamorphism. The metamorphic temperature experienced by Kainsaz (CO3.1) places an upper limit on the temperature experienced in the parent body by the CO3 chondrites we studied. Both CO3 chondrites and unequilibrated ordinary chondrites (UOCs) exhibit metamorphic sequences (Huss et al., 1981; Sears et al., 1991a, 1991b). Huss and Lewis (1994b) estimated a temperature of ~300°C for Bishunpur (L3.1). However, Sears et al. (1991b) argue that CO3s spent longer times at lower temperatures than did the UOCs. If so, then 300°C is a hard upper limit for the temperature experienced by Kainsaz on its parent body.

The relative abundances of the three noble-gas components in diamonds provide additional temperature information, and CO3 diamonds tell a complicated story. The Xe-P3 release patterns for the diamonds in ALHA77307 and Colony (Fig. 1) are much like that for Semarkona (LL3.0) diamonds (Huss and Lewis, 1994b) and appear to represent diamonds that have been heated only to ~200°C. This is consistent with the absence of metamorphic effects in silicates at the micron scale in ALHA77307 and Colony (Scott and Jones, 1990), and implies a metamorphic temperature of ~200°C. However, ALHA 77307 and Colony diamonds have only ~75 and ~50%, respectively, of the Xe-P3 in Semarkona diamonds. The refractory Xe-P6 component for ALHA77307 and Colony diamonds are 17 and 34%, respectively, higher than in Semarkona diamonds (cf. Huss and Lewis, 1994b). Thus, in contrast to the Xe-P3 release patterns, the abundances of Xe-P3 and Xe-P6 imply that CO3 diamonds have seen a significantly higher

temperature than Semarkona diamonds. These contradictory observations can be reconciled if CO3 diamonds are mixtures of low-temperature diamonds containing significant Xe-P3 and high-temperature diamonds that have lost their Xe-P3 and some Xe-HL, and are thus enriched in Xe-P6. A mixture of 25% Xe-P3-free diamonds such as those found in type 3.5 ordinary chondrites or in Allende (CV3) and 75% Semarkona-like diamonds gives a good match to ALHA77307 diamonds (data from Huss and Lewis, 1994b). A slightly better match is obtained with a low-*T* component ~5% more enriched in Xe-P3 than Semarkona diamonds. For Colony, a 50%-50% mixture gives a good match, and a slightly better match is obtained with low-*T* diamonds slightly less Xe-P3-rich than Semarkona diamonds. The temperature experienced by the high-*T* component is hard to constrain. The diamond data constrain the temperature to be > 300°C and < ~550°C in a relatively oxidizing environment like CO3 chondrites (Huss and Lewis, 1994b).

Silicon carbide abundances also imply mixtures of two components. Matrix-normalized silicon carbide abundances for ALHA77307 and Colony are ~62% and ~26% of that in Orgueil (Table 7). Comparisons with ordinary chondrites predict that material heated to 450°C would have < 10% of its original silicon carbide. Renazzo matrix, which we estimated to have been heated to 400 to 450°C, has ~13% of its silicon carbide remaining. In contrast, material heated to only ~200°C should have ~70% of its silicon carbide remaining (cf. Huss and Lewis, 1995). Using Semarkona-like material as the low-*T* end member and material with ~15% silicon carbide as the high-*T* end member, a mixture of 85% low-*T* plus 15% high-*T* components will match ALHA77307. The calculated mixture can be made consistent with the diamond mixture for ALHA77307 by increasing the silicon carbide content of the low-*T* component to ~82% of the amount in Orgueil. Thus, both the diamond components and the silicon carbide abundance suggest a low-*T* component in ALHA77307 that was heated slightly less than Semarkona matrix. Survival of minor graphite in ALHA77307 (Table 7) is consistent with this inference. For Colony, a mixture of 33% low-*T* plus 67% high-*T* components like those used for ALHA77307 matches reasonably well, but a better match with the 50 to 50% mixture estimated from diamonds is obtained if the low-*T* component has about half the silicon carbide in Semarkona.

Taken together, the abundance data imply that ALHA77307 matrix is a mixture of ~75% material that was heated less than Semarkona matrix (≤200°C) and 25% material that was heated to ~400°C. Thus the metamorphic temperature experienced by ALHA77307 in its parent body was also ≤200°C. Colony appears to be a mixture of 50% high-*T* and 50% low-*T* components, with the low-*T* component heated slightly more than the low-*T* component in ALHA77307. The higher temperature for the low-*T* component in Colony could reflect parent-body processing; it is not possible using presolar grains to distinguish between nebula and parent-body processing for the lowest-temperature material.

The bulk compositions are consistent with addition of a low-*T* component after the peak processing temperature was reached in the CO3 compositional region. The enrichments of gold through nickel in the CO3 bulk compositions indicate that the main reservoir of CO3 material from which chondrules formed had been processed to a temperature somewhat less than the CR2 precursors (perhaps 400°C) before chondrule formation. Mixing calculations assuming high-*T* and low-*T* matrix components as described above totaling 33% of the meteorite, chondrules produced from the high-*T* component (65%), and 2% CAIs enriched to ~25 × CI in refractory elements can roughly reproduce the observed enrichments of refractory elements for Colony, Kainsaz, and average CO3 (Fig. 5a). The lower enrichments of refractory elements and the higher proportion of low-*T* material inferred for ALHA77307 matrix suggest that ALHA77307 acquired much more of the low-*T* matrix component than most CO3 chondrites.

4.2.3. CV3 Chondrites

Figures 6 and 7 compare the bulk compositions and abundances of presolar components for reduced and oxidized CV3 chondrites to those of Orgueil. The bulk compositions of both groups show evidence of more-severe thermal processing than either CR or CO chondrites. Elements more refractory than calcium are enriched by a factor of two compared to Orgueil, reflecting in part a higher abundance of CAIs in CV chondrites (4–9%, McSween, 1977a). However, magnesium, which dominantly resides in chondrules and is part of the suite used above to monitor the dominant refractory component in the bulk meteorites, is enriched by 50% compared to Orgueil (vs. 40–43% and 30–35% for CR and CO, respectively). In addition, lithophile elements show increasing relative depletions as a function of volatility starting with vanadium, rather than manganese, and siderophile elements show relative depletions starting with nickel and cobalt, rather than gold. Note that refractory siderophiles are systematically depleted relative to refractory lithophiles in both reduced and oxidized CVs, consistent with mechanical separation of metal and silicate (e.g., Larimer and Anders, 1970), perhaps initiated by chondrule formation (Connolly et al., 2001). However, volatile siderophiles may be somewhat enriched relative to volatile lithophiles, perhaps implying partial re-condensation of these elements.

Presolar components also indicate higher nebula temperatures. Reduced CV3s have higher diamond abundances and their diamonds have higher Xe-P6 contents compared to Orgueil, while other components are relatively depleted (Fig. 6b). The abundance pattern is a monotonic function of volatility, except for slightly higher Xe-P3/Xe-HL ratios than one might expect from the trend in Renazzo (cf. Fig. 4b). Somewhat lower abundances for Vigarano ($CV3.3_{red}$) of Xe-P1, silicon carbide, and Xe-P3 in diamonds relative Leoville ($CV3.0_{red}$) (petrologic types from Guimon et al., 1995) may reflect parent-body metamorphism. However, the release of Xe-P3 peaks at ~750°C in both Leoville and Vigarano, much like the patterns in Semarkona and Bishunpur (Huss and Lewis, 1994b). Huss and Lewis (1994b) suggested that diamonds from Leoville and Vigarano are mixtures of a low-*T* component that was heated to no more than ~300°C and a high-*T* component heated to > 450°C. Bulk compositions indicate that the high-*T* component in CV3 chondrites reached higher temperatures than CR and CO chondrites, perhaps 500 to 600°C (but see below). This interpretation implies that the high-*T* component in both meteorites had lost essentially all of its silicon carbide and some of its Xe-P1, and that the Xe-P3-rich diamonds, the silicon car-

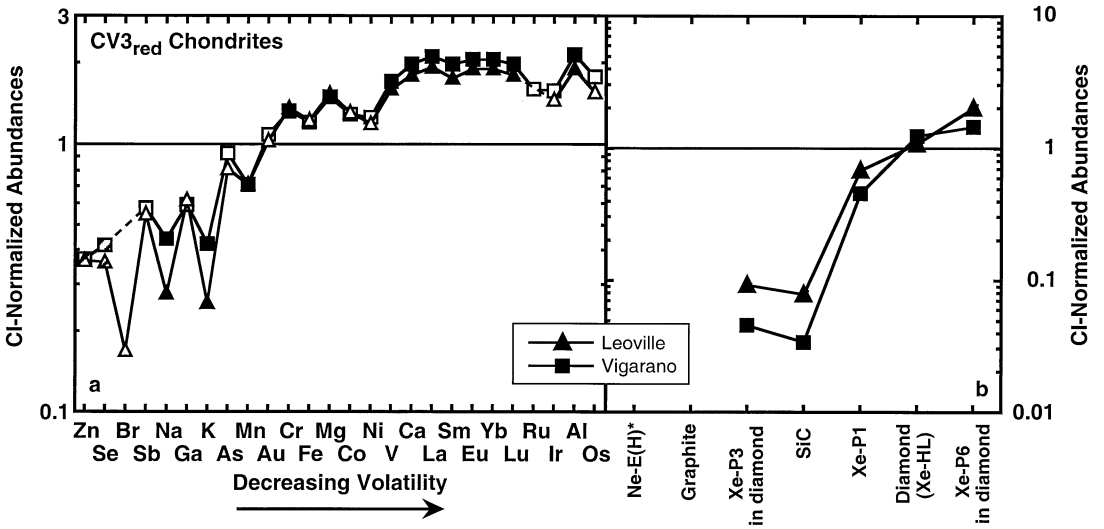

Fig. 6. Bulk compositional data and abundances of presolar components are shown for the reduced CV3s, Leoville and Vigarano. Plotting conventions follow previous Figures. (a) Refractory lithophiles are enriched 2x relative to CI chondrites, vanadium, magnesium, and chromium show volatility-dependent enrichments relative to CI, and the more volatile elements are depleted. Refractory and moderately volatile siderophile elements are depleted relative to lithophile elements, but volatile siderophiles appear to be enriched. The large depletions of bromine, sodium, and potassium for Leoville, a find from Kansas, probably reflect terrestrial weathering. (b) Presolar diamond and Xe-P6 in diamond are enriched relative to CI, but Xe-P1, SiC, and Xe-P3 in diamond are depleted. No evidence of presolar graphite or oxidizable Ne-E(H)* was found. Bulk compositional data are from Kallemeyn and Wasson (1981) and Kracher et al. (1985). Abundance data for Leoville and Vigarano are from Huss and Lewis (1994a, 1994b, 1995).

bide, and a portion of the Xe-P1 were supplied by the low-*T* component. In this interpretation, the differences between Leoville and Vigarano primarily reflect different mixing ratios between the low- and high-*T* components, not metamorphism.

Although the bulk compositions of oxidized CV3s show the same characteristics as reduced CV3s, the presolar components show some differences (Figs. 6 and 7). As in reduced CV3s, the Xe-P6 abundances for Mokoia, Axtell, and Allende diamonds

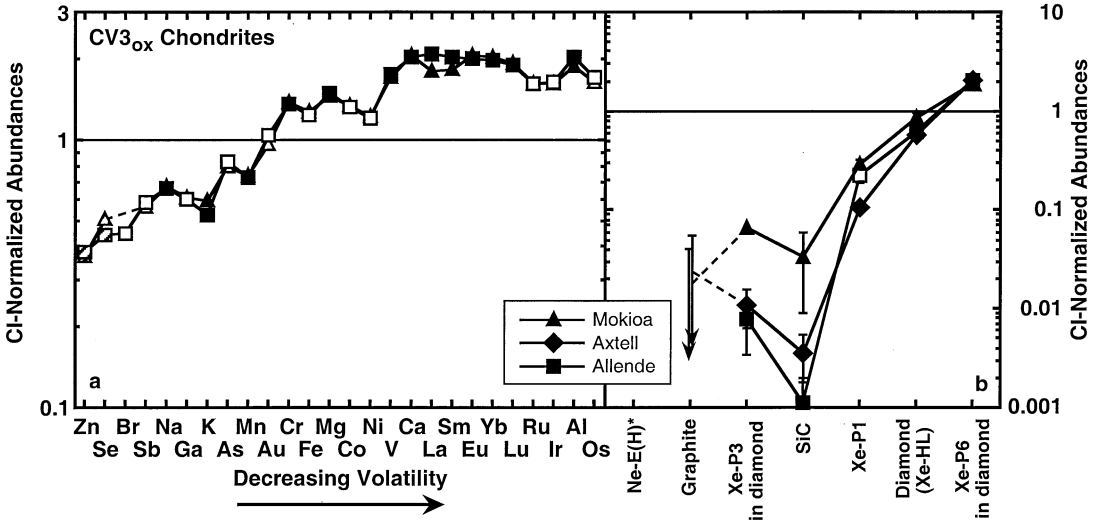

Fig. 7. Bulk compositional data for Mokoia and Allende and abundances of presolar components for Mokoia, Axtell, and Allende, all oxidized CV3s, are shown. Plotting conventions follow previous Figures. (a) Refractory lithophiles are enriched 2 × relative to CI chondrites, vanadium, magnesium, and chromium show volatility-dependent enrichments relative to CI, and the more volatile elements are depleted. Refractory and moderately volatile siderophile elements are depleted relative to lithophile elements, but volatile siderophiles appear to be enriched. (b) Xe-P6 in diamond is enriched relative to CI, but abundances of diamond, Xe-P1, SiC, and Xe-P3 in diamond are depleted. No evidence of presolar graphite or oxidizable Ne-E(H)* was found. SiC abundances for Axtell and Mokoia (open diamond and triangle) are a lower limits (see text). Bulk compositional data are from Kallemeyn and Wasson (1981). Most abundance data for Allende are from Huss and Lewis (1994a, 1994b, 1995). Xe-P1 (open square) was estimated from residues 3C1 and 3CS1 from Lewis et al. (1975).

are enriched by a factor of two relative to Orgueil. But, the matrix-normalized diamond abundances are lower than in Orgueil, and the diamond, Xe-P1, and silicon carbide abundances are lower than in reduced CV3s (note scale in Fig. 7b). The Xe-P3 contents of Axtell and Allende diamonds are significantly lower, but diamonds in Mokoia and Leoville have similar Xe-P3 contents (Figs. 6b and 7b). Abundances generally decrease from Mokoia to Axtell to Allende, consistent with independent evidence of increasing degree of parent body metamorphism (McSween, 1977a; Krot et al., 1995; Simon et al., 1995). However, this sequence does not correspond to the petrologic subtypes based on TL sensitivity (Mokoia 3.2, Axtell 3.0, Allende 3.2; Guimon et al., 1995). The reasons are not clear, but may reflect differences in the style of secondary alteration.

A striking difference between oxidized and reduced CV3s is the degree to which constituents of oxidized CV3s have been metasomatized (Krot et al., 1995). In Allende and Axtell, the CAIs, chondrules, and matrix have experienced moderate iron-alkali-halogen metasomatism. In the CAIs, metasomatism converted primary CAI minerals to anorthite, grossular, nepheline, sodalite, hedenbergite, and poorly characterized alumino-silicates; in chondrules, it converted olivines to fayalite along their edges and along cracks, sulfidized and oxidized metal grains, and replaced mesostasis with secondary minerals or stripped the mesostasis of reactive components; in the matrix, it replaced low-Ca pyroxene with fayalite and added nepheline and sodalite to the matrix assemblage (Krot et al., 1995; Srinivasan et al., 2000). Metasomatism is extensive in most oxidized CV3s, but a mild version also affected components of the reduced CV3s. The temperature at which this metasomatism occurred has been variously estimated at between 500 and 1200°C, though most authors favor temperatures at the low end of this range (e.g., Krot et al., 1995). In Mokoia, the dominant alteration phases are phyllosilicates, which are found in CAIs, chondrules, and matrix. The temperatures at which the phyllosilicates formed are variously estimated at between 75 and 200°C, although the temperature is not at all well constrained. Cross-cutting relationships exhibited in Bali ($CV3_{ox}3.0$) indicate that aqueous alteration took place on the parent body (see summary in Krot et al., 1995). Some CAIs in Mokoia contain secondary anorthite and grossular in addition to phyllosilicate. However, it has not been determined whether or not the constituents of Mokoia, Kaba, and other meteorites with extensive phyllosilicate replacement were subjected to the same degree of metasomatism experienced by Axtell and Allende before aqueous alteration.

Our data may help to sort out this issue. All oxidized CV3s are depleted in diamond, Xe-P1, and silicon carbide relative to reduced CV3 chondrites. This implies that oxidized CV3s have been exposed to more-severe processing than reduced CV3s. Aqueous alteration is probably not the explanation. Aqueous processes on the parent bodies do not seem to result in destruction of diamonds, silicon carbide, and the P1 carrier (cf. CI and CM2 chondrites). The relatively lower abundances of diamond, silicon carbide, and the P1 carrier are so far confined to the oxidized CV3s, and destruction of these components requires moderately high temperatures. This implicates the metasomatism that produced the oxidized CV3s as the cause of the lower abundances. Mokoia diamonds have a Xe-P3 content similar to that in Leoville diamonds. Mokoia also contains a small amount of very deuterium-rich organic material such as that found in Renazzo and to a lesser extent in CI and CM2 chondrites (Kolodny et al., 1980). Similar material is apparently not present in Allende (Yang and Epstein, 1983). These observations suggest that constituents of Mokoia first underwent the same metasomatic event as other oxidized CV3s, altering the chondrules, CAIs, and matrix, and reducing the abundances of diamond, silicon carbide, and Xe-P1, and then later, Mokoia acquired a small amount of low-temperature material, which included water-bearing phases, Xe-P3-bearing diamonds, silicon carbide, and deuterium-enriched organics. One might also expect Mokoia to contain presolar graphite, but the high abundance of solar gas and the loss of the 800°C step did not permit us to detect any. Aqueous alteration then took place on the parent body at temperatures < 200°C to produce the meteorite we see today. We cannot tell conclusively whether the metasomatism occurred before or after accretion. But two stages of alteration in Mokoia, moderately high-temperature metasomatism followed by relatively low-temperature aqueous alteration suggest two separate sites. Axtell and Allende may or may not have acquired the low-temperature material. The high concentration of solar gases in Mokoia suggests that it was on the surface of its parent body. Perhaps the low-temperature, water-bearing material was added only in the final stages of accretion of the CV3 parent body. Axtell and Allende may have been buried deeply enough not to acquire the low-temperature component. However, these meteorites were probably heated to temperatures on the parent body high enough to effectively eliminate the low-temperature components (estimates range up to 500–600°C; e.g., Krot et al., 1995).

Thus, the bulk compositional data and abundances of presolar components indicate that the CV precursors were heated to higher temperatures in the nebula than either CR or CO chondrites, perhaps 500 to 600°C. This processing removed volatile elements and labile presolar components, resulting in higher abundances of refractory components in the remaining solids. After chondrule and CAI formation, and probably after metal-silicate fractionation, oxidized CVs experienced additional moderate metasomatism, which further depleted the presolar components. Before or during accretion, some lightly processed dust was added back into the matrices of both reduced and oxidized CV3 chondrites. Parent-body metamorphism probably destroyed evidence of this component in Axtell and Allende.

4.2.4. CH Chondrites

Figure 8 shows the bulk compositional data for Acfer 214 and average CH chondrites and the abundances of presolar components in Acfer 214, normalized to CI chondrites. The most obvious feature in the bulk composition is the very large enrichment in siderophile elements relative to lithophile elements. The siderophile elements more refractory than cobalt are not fractionated from one another, but the more-volatile siderophiles show increasing depletions with increasing volatility. Lithophile elements more refractory than chromium have a relatively flat pattern and are enriched relative to CI. The degree of enrichment due to depletion of volatiles is masked by

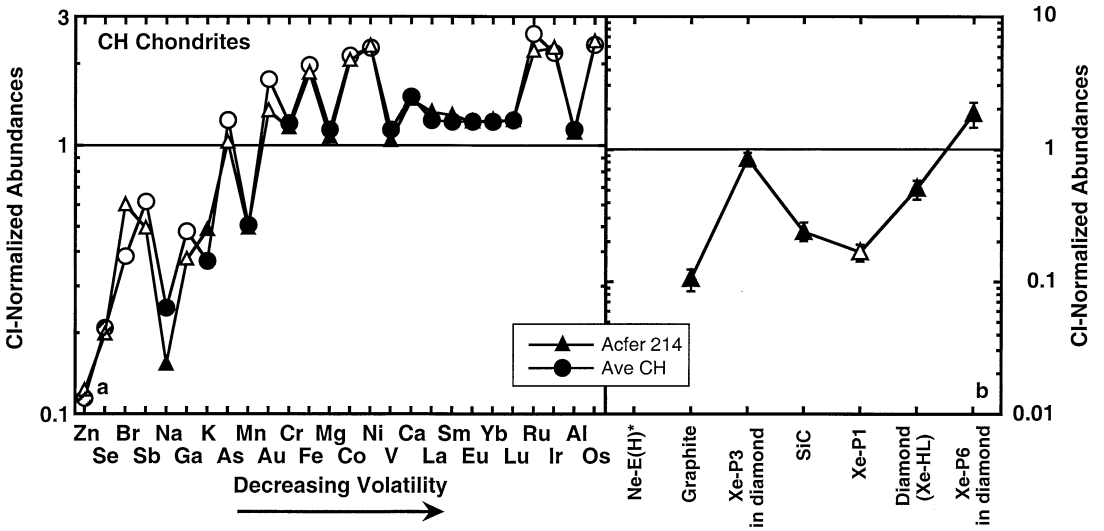

Fig. 8. Bulk compositional data for Acfer 214 and average CH chondrites and abundances of presolar components for Acfer 214 are shown. Plotting conventions follow previous Figures. (a) Siderophile elements are strongly enriched relative to lithophile elements and show relative volatility-dependent depletions for elements more volatile than cobalt. Lithophile elements more refractory than chromium are unfractionated and enriched relative to CI, while volatile lithophiles show volatility-dependent depletions. (b) Acfer 214 shows high abundances of graphite, SiC, and Xe-P3 in diamonds as well as a large enrichment in Xe-P6 in diamond relative to CI. These abundances reflect a mixture of high- and low-temperature components (see text). The Xe-P1 abundance (open triangle) may be too low due to terrestrial weathering (see text). Bulk compositional data from Bischoff et al. (1993).

the large enrichment of siderophiles elements. The abundances of presolar grains show a very unusual pattern. Xe-P6 in diamonds is enriched by nearly a factor of two relative to Orgueil diamonds, but Xe-P3 is ~75% of the amount in CI diamonds (Fig. 1). The release pattern of Xe-P3 is very similar to that for CI and CM2 diamonds. These characteristics clearly indicate a mixture of highly processed diamonds, in which the Xe-P6 carrier is highly enriched, and unprocessed diamonds with a full complement of Xe-P3. The abundances of graphite, silicon carbide, diamonds, and Xe-P1 are lower than those in CI chondrites. Acfer 214 is a weathered "desert" meteorite and the weathering may well have released some of the Xe-P1 (cf. Huss et al., 1996), so we will not consider Xe-P1 further. The matrix-normalized graphite and silicon carbide abundances are only ~10 and ~25%, respectively, of the abundances in Orgueil. If the high-*T* component were devoid of silicon carbide, this would imply that the unprocessed low-*T* component makes up ~25% of the matrix of Acfer 214. This would seem to be at odds with a Xe-P3 content in diamonds 75% of that in Orgueil. However, Acfer 214 also contains ~3% dark inclusions made up of matrix-like material and rich in sulfides. If these inclusions were carriers of silicon carbide, then the silicon carbide content in the inclusions would be very similar to that in Orgueil. The diamonds might also be carried in the inclusions. Because Xe-P3-rich diamonds contain ~65% of the Xe-HL concentration found in Xe-P3-depleted diamonds, the Xe-P3-rich diamonds would carry about half of the Xe-HL in Acfer 214. If all of the Xe-P3-rich diamonds were in the dark inclusions, then the inclusions would have a diamond abundance very similar to that in Orgueil (1440 ppm). The graphite abundance of the inclusions would only be ~4.3 ppm, compared to 10 ppm for Orgueil. This may reflect the presence of solar gases in the low-temperature gas from Acfer 214, which masks Ne-E(L) and results in an underestimate of the graphite abundance. Thus, Acfer 214 seems to be a mixture of metal that has been processed to relatively high temperature, depleting elements more volatile than cobalt, silicates that have been processed to somewhat lower temperature (400–450°C), but still hot enough to destroy silicon carbide and most of the diamonds (some of this component was processed into chondrules), and dark inclusions that are samples of thermally unprocessed bulk dust from the sun's parent molecular cloud. The survival of Xe-P3 and graphite requires that the bulk meteorite was never subjected to temperatures above 100 to 150°C after accretion.

4.3. Relationships Among Chondrite Groups

We have shown above that abundances of presolar grains and bulk compositional characteristics of chondrites are closely related. This is most easily understood if the nebular processing that produced the chondrite groups was the same as that which modified the initial inventory of presolar grains. The idea that the compositional groups were produced before chondrules formed has been around for some time (e.g., Grossman and Wasson, 1983). Remarkably, the presolar grains seem to provide an independent way to monitor the extent of nebular processing of chondrule and chondrite precursors. It is important to note that the correlations between abundances of presolar grains and the bulk compositional characteristics of chondrites *rule out* differential condensation from a gaseous nebula of solar composition as the dominant mechanism for producing the compositional characteristics of chondrites. The grains all would have been destroyed if the nebula was entirely vaporized.

The bulk compositional and presolar grains data make sense

in the following framework. All of the chondrites, carbonaceous and otherwise, formed from the same bulk reservoir, the presolar dust inherited from the Sun's parent molecular cloud. This parent material was heated to different degrees in the nebula before chondrule formation and accretion, producing the basic chemical characteristics of the different chondrite groups. Chondrules then formed, mechanical mixing of components and, in some cases, metal-silicate fractionation took place, meteorite parent bodies accreted, and parent-body processes further altered the material. Several different levels of nebular processing are represented by the carbonaceous chondrites. The least-processed, least-fractionated material now occurs as the CI chondrites and as the matrices of CM2 chondrites. Low-T components processed to no more than 200 to 300°C are found in CO3 and CV3 chondrites. The high-*T* components in carbonaceous chondrites can be placed in the following order, from lowest to highest temperature: CO $<$ CR $\approx$ CH $<$ CV. These relationships are summarized in Table 8. Note that the bulk compositional data indicate that the chondrule component in CM2 chondrites was processed to a similar degree as the COs before chondrule formation (Figs. 2 and 5). The fine-grained high-*T* component in CM2 chondrites has been swamped by the CI-like material that dominates the matrix, but may still be visible as slight excesses of Xe-P1 in CM2 matrices and Xe-P6 in CM2 diamonds (Fig. 3).

Other classes of chondrites fit into the same picture and will be discussed in detail in a subsequent paper. However, comparisons of the data from this paper and data from Huss and Lewis (1995) indicate that ordinary chondrites fall between CI and CO chondrites, and that EH chondrites, which were processed in a highly reducing environment, may have been heated as much as CV chondrites. Because the carbonaceous chondrites apparently span the range of intensity of nebular processing recorded in chondrites, it may be counterproductive to think of carbonaceous chondrites as a group distinct from other types of chondrites.

4.4. Quantification of Nebular Temperatures

There may be some large systematic uncertainties in the temperatures derived above for the nebular processing, particularly for the high-*T* processing. Temperatures for low-*T* processing are derived primarily from Xe-P3 in diamonds and should be reliable. Huss and Lewis (1994a) argue that release of P3 gases occurs via a structural re-organization of the diamond surface layers. This re-organization occurs at temperatures below those required to initiate most chemical reactions and thus P3 release is largely independent of the surroundings (Huss and Lewis, 1994b). The P3 release temperatures are calibrated both from mineralogical indicators in the matrices of unequilibrated ordinary chondrites and by release in the mass spectrometer inlet system during both pyrolysis and oxidation experiments. The temperatures for high-*T* processing are much less certain. They are based primarily on destruction of diamond, silicon carbide, and deuterium-rich organics under metamorphic conditions on meteorite parent bodies. An independent temperature calibration comes from an extensive set of experiments on the kinetics of SiC destruction under nebular conditions performed by Mendybaev et al. (2002). Their work implies that temperatures of $\geq$ 700°C are required to efficiently destroy SiC under a variety of fO_2 conditions in the solar nebula. This is considerably hotter than the temperatures inferred above, but is more in line with the 50% equilibrium condensation temperatures of elements like gold and manganese, the most refractory elements to be depleted in the bulk compositions (e.g., Wasson, 1985). Thus, we may have underestimated the temperatures of nebular processing by as much as 300°C, but we are confident that the relative temperature scale derived for the carbonaceous chondrites is correct.

5. SUMMARY AND CONCLUSIONS

We have determined abundances of presolar diamond, silicon carbide, graphite, and Xe-P1 in the Murchison (CM2), Murray (CM2), Renazzo (CR2), ALHA77307 (CO3.0), Colony (CO3.0), Mokoia (CV_{ox}), Axtell (CV_{ox}),and Acfer 214 (CH) chondrites. These data, combined with data obtained previously by Huss and Lewis (1995), provide a reasonably comprehensive data set of presolar grain abundances in carbonaceous chondrites. The abundance data together with bulk compositional data for the host meteorites permit detailed comparisons to be made between chondrite classes. We showed that the chemical fractionations recorded in the bulk compositions and the abundance patterns of the presolar grains are correlated across the carbonaceous chondrites. This indicates that the same nebular processing that produced the bulk compositions of the chondrite classes from the material inherited from the sun's parent molecular cloud also modified the assemblage of presolar grains in each class. If so, then the various chondrite classes were not produced by various degrees of condensation from a gas of solar composition, because the presolar grains would not have survived to record the processing. Instead, nebula processing primarily involved different levels of heating of presolar dust, with chondrule formation, metal-silicate fractionation, and perhaps local condensation superimposed on the resulting materials.

Our analysis shows that carbonaceous chondrites span the range of nebular processing recorded in chondrites. Some accreted relatively unprocessed molecular-cloud dust (CI, CM matrix). Others reflect relatively simple thermal processing to moderate temperature (e.g., CR). Some are dominated by material that was heavily processed in the nebula (e.g., CV). And several contain both highly processed and nearly unprocessed materials (CM, CO, CV, CH). Metal-silicate fractionation is recorded in some carbonaceous chondrites (CV, CH). The carbonaceous chondrites are at least as different from each other as they are from ordinary and enstatite chondrites. These differences must be appreciated when discussing the characteristics and history of individual meteorites and when comparing "carbonaceous" chondrites to other chondrite groups.

Acknowledgments—This work was supported by NASA grants NAG5-8173, NAG5-10449, and NAG5-11770 (GRH) and NAG5-9414 (CMH). We thank the Center for Meteorite Studies at ASU, the Naturhistorisches Museum in Vienna, G. J. Wasserburg, and the Antarctic Meteorite Curatorial Facility for providing samples for this study. Reviews by Roy Lewis, Jamie Gilmour, Monica Grady, and an anonymous reviewer resulted in significant improvements to this paper.

Associate editor: M. M. Grady

REFERENCES

Alaerts L., Lewis R. S., and Anders E. (1979) Isotopic anomalies of noble gases in meteorites and their origins—IV. CO3 (Ornans) carbonaceous chondrites. *Geochim. Cosmochim. Acta* **43,** 1421–1432.

Amari S., Anders E., Virag A., and Zinner E. (1990) Interstellar graphite in meteorites. *Nature* **345,** 238–240.

Amari S., Lewis R. S., and Anders E. (1994) Interstellar grains in meteorites: I. Isolation of SiC, graphite, and diamond; size distributions of SiC and graphite. *Geochim. Cosmochim. Acta* **58,** 459–470.

Amari S., Lewis R. S., and Anders E. (1995) Interstellar grains in meteorites: III. Graphite and its noble gases. *Geochim. Cosmochim. Acta* **59,** 1411–1426.

Anders E. and Grevesse N. (1989) Abundances of the elements: Meteoritic and solar. *Geochim. Cosmochim. Acta* **53,** 197–214.

Bischoff A., Palme H., Schultz L., Weber D., Weber H. W., and Spettel B. (1993) Acfer 182 and paired samples, an iron-rich carbonaceous chondrite: Similarities with ALH85085 and relationship to CR chondrites. *Geochim. Cosmochim. Acta* **57,** 2631–2648.

Choi B.-G., Huss G. R., Wasserburg G. J., and Gallino R. (1998) Presolar corundum and spinel in ordinary chondrites: Origins from AGB stars and a supernova. *Science* **282,** 1284–1289.

Choi B.-G., Wasserburg G. J., and Huss G. R. (1999) Circumstellar hibonite and corundum and nucleosynthesis in asymptotic giant branch stars. *Astrophys. J.* **522,** L133–L136.

Connolly H. C., Jr., Huss G. R., and Wasserburg G. J. (2001) On the formation of Fe-Ni metal in Renazzo-like carbonaceous chondrites. *Geochim. Cosmochim. Acta* **65,** 4567–4588.

Dauphas N., Marty B., and Reisberg L. (2002) Molybdenum nucleosynthetic dichotomy revealed in primitive meteorites. *Astrophys. J.* **569,** L139–L142.

Eberhardt P., Eugster O., and Marti K. (1965) A redetermination of the isotopic composition of atmospheric neon. *Z. Naturforsch.* **20a,** 623–624.

Geiss J., Buehler F., Cerutti H., Eberhardt P., and Filleaux C. H. (1972) Solar wind composition experiments. In *Apollo 15 Preliminary Scientific Report*, chap. 15.

Grossman J. N. and Wasson J. T. (1983) The compositions of chondrules in unequilibrated chondrites: An evaluation of models for the formation of chondrules and their precursors. In *Chondrules and Their Origins* (ed. E. A. King), pp. 88–121. Lunar and Planetary Institute, Houston, TX.

Grossman L. and Olsen E. (1974) Origin of the high-temperature fraction of C2 chondrites. *Geochim. Cosmochim. Acta* **38,** 173–187.

Guimon R. K., Symes S. J. K., Sears D. W. G., and Benoit P. H. (1995) Chemical and physical studies of type 3 chondrites XII: The metamorphic history of CV chondrites and their components. *Meteoritics* **30,** 704–714.

Halbout J., Robert F., and Javoy M. (1990) Hydrogen and oxygen isotope compositions in kerogen from the Orgueil meteorite: Clues to a solar origin. *Geochim. Cosmochim. Acta* **54,** 1453–1462.

Huss G. R. (1990) Ubiquitous interstellar diamond and SiC in primitive chondrites: Abundances reflect metamorphism. *Nature* **347,** 159–162.

Huss G. R. (1997) The survival of presolar grains in solar system bodies. In *Astrophysical Implications of the Laboratory Study of Presolar Materials* (eds. T. J. Bernatowicz and E. Zinner), pp. 721–748. American Institute of Physics, New York.

Huss G. R. and Alexander E. C., Jr. (1987) On the presolar origin of the "normal planetary" noble gas component in meteorites. *J. Geophys. Res.* **92,** *(Suppl)*, E710–E716.

Huss G. R. and Lewis R. S. (1994a) Noble gases in presolar diamonds I: Three distinct components and their implications for diamond origins. *Meteoritics* **29,** 791–810.

Huss G. R. and Lewis R. S. (1994b) Noble gases in presolar diamonds II: Component abundances reflect thermal processing. *Meteoritics* **29,** 811–829.

Huss G. R. and Lewis R. S. (1995) Presolar diamond, SiC, and graphite in primitive chondrites: Abundances as a function of meteorite class and petrologic type. *Geochim. Cosmochim. Acta* **59,** 115–160.

Huss G. R., Keil K., and Taylor G. J. (1981) The matrices of unequilibrated ordinary chondrites: Implications for the origin and history of chondrites. *Geochim. Cosmochim. Acta* **45,** 33–51.

Huss G. R., Fahey A. J., Gallino R., and Wasserburg G. J. (1994) Oxygen isotopes in circumstellar Al_2O_3 grains from meteorites and stellar nucleosynthesis. *Astrophys. J. Lett.* **425,** L81–L84.

Huss G. R., Lewis R. S., and Hemkin S. (1996) The "normal planetary" noble gas component in primitive chondrites: Compositions, carrier, and metamorphic history. *Geochim. Cosmochim. Acta* **60,** 3311–3340.

Hutcheon I. D., Huss G. R., Fahey A. J., and Wasserburg G. J. (1994) Extreme ^{26}Mg and ^{17}O enrichments in an Orgueil corundum: Identification of a presolar oxide grain. *Astrophys. J. Lett.* **425,** L97–L100.

Ireland T. R. (1990) Presolar isotopic and chemical signatures in hibonite-bearing refractory inclusions from the Murchison carbonaceous chondrite. *Geochim. Cosmochim. Acta* **54,** 3219–3237.

Kallemeyn G. W. and Wasson J. T. (1981) The compositional classification of chondrites—I. The carbonaceous chondrite groups. *Geochim. Cosmochim. Acta* **45,** 1217–1230.

Kallemeyn G. W. and Wasson J. T. (1982) The compositional classification of chondrites: III. Ungrouped carbonaceous chondrites. *Geochim. Cosmochim. Acta* **46,** 2217–2228.

Kallemeyn G. W., Rubin A. E., and Wasson J. T. (1994) The compositional classification of chondrites: VI. The CR carbonaceous chondrite group. *Geochim. Cosmochim. Acta* **58,** 2873–2888.

Kerridge J. F. (1983) Isotopic composition of carbonaceous-chondrite kerogen: Evidence for an interstellar origin of organic matter in meteorites. *Earth Planet. Sci. Lett.* **64,** 186–200.

Kolodny Y., Kerridge J. F., and Kaplan I. R. (1980) Deuterium in carbonaceous chondrites. *Earth Planet. Sci. Lett.* **46,** 149–158.

Kracher A., Keil K., Kallemeyn G. W., Wasson J. T., Clayton R. N., and Huss G. I. (1985) The Leoville (CV3) accretionary breccia. *J. Geophys. Res.* **90, (***Suppl***)**, D123–D135.

Krähenbühl U., Morgan J. W., Ganapathy R., and Anders E. (1973) Abundance of 17 trace elements in carbonaceous chondrites. *Geochim. Cosmochim. Acta* **37,** 1353–1370.

Krot A. N., Scott E. R. D., and Zolensky M. E. (1995) Mineralogical and chemical modification of components in CV3 chondrites: Nebular or asteroidal processing. *Meteoritics* **30,** 748–775.

Larimer J. W. and Anders E. (1970) Chemical fractionations in meteorite—III. Major element fractionations in chondrites. *Geochim. Cosmochim. Acta* **34,** 367–387.

Lewis R. S., Srinivasan B., and Anders E. (1975) Host phase of a strange xenon component in Allende. *Science* **190,** 1251–1262.

Lewis R. S., Tang M., Wacker J. F., Anders E., and Steel E. (1987) Interstellar diamonds in meteorites. *Nature* **326,** 160–162.

Lewis R. S., Amari S., and Anders E. (1994) Interstellar grains in meteorites. II. SiC and its noble gases. *Geochim. Cosmochim. Acta* **58,** 471–494.

McCoy T. J., Keil K., Ash R. D., Morse A. D., Pillinger C. T., Wieler R., Mayeda T. K., Clayton R. N., Benoit P. H., Sears D. W. G., Casanova I., Muenow D. W., Moore C. B., Lewis C. F., and Wilson I. E. (1993) Roosevelt County 075: A petrologic, chemical and isotopic study of the most unequilibrated known H chondrite. *Meteoritics* **28,** 681–691.

McSween H. Y., Jr. (1977a) Petrographic variations among carbonaceous chondrites of the Vigarano type. *Geochim. Cosmochim. Acta* **41,** 1777–1790.

McSween H. Y., Jr. (1977b) Carbonaceous chondrites of the Ornans type: A metamorphic sequence. *Geochim. Cosmochim. Acta* **41,** 477–491.

McSween H. Y., Jr. (1979) Alteration in CM carbonaceous chondrites inferred from modal and chemical variations in matrix. *Geochim. Cosmochim. Acta* **43,** 1761–1770.

Mendybaev R. A., Beckett J. R., Grossman L., Stolper E., Copper R. F., and Bradley J. P. (2002) Volatilization kinetics of silicon carbide in reducing gases: An experimental study with applications to the survival of presolar grains in the solar nebula. *Geochim. Cosmochim. Acta* **66,** 661–682.

Messenger S., Keller L. P., Stadermann F. J., Walker R. M., and Zinner E. (2003) Samples of stars beyond the solar system: Silicate grains in interplanetary dust. *Science* **300,** 105–108.

Nier A. O. (1950) A redetermination of the relative abundances of the isotopes of neon, krypton, rubidium, xenon, and mercury. *Phys. Rev.* **79,** 450–454.

Nittler L. R., Alexander C. M. O'D., Gao X., Walker R. M., and Zinner E. K. (1994) Interstellar oxide grains from the Tieschitz ordinary chondrite. *Nature* **370,** 443–446.

Nittler L. R., Hoppe P., Alexander C. M. O'D., Amari S., Eberhardt P., Gao X., Lewis R. S., Strebel R., Walker R. M., and Zinner E. (1995) Silicon nitride from supernovae. *Astrophys. J.* **453,** L25–L28.

Nittler L. R., Alexander C. M. O'D., Gao X., Walker R. M., and Zinner E. K. (1997) Stellar sapphires: The properties and origin of presolar Al_2O_3 in meteorites. *Astrophys. J.* **483,** 475–495.

Podosek F. A., Ott U., Brannon J. C., Neal C. R., Bernatowicz T. J., Swan P., and Mahan S. E. (1997) Thoroughly anomalous chromium in Orgueil. *Meteorit. Planet. Sci.* **32,** 617–627.

Rees C. E. (1984) Error propagation calculations. *Geochim. Cosmochim. Acta* **48,** 2309–2311.

Robert F. and Epstein S. (1982) The concentration and isotopic composition of hydrogen, carbon and nitrogen in carbonaceous meteorites. *Geochim. Cosmochim. Acta* **46,** 81–95.

Rubin A. E., James J. A., Keck B. D., Weeks K. S., Sears D. W. G., and Jarosewich E. (1985) The Colony meteorite and variations in CO3 chondrite proportions. *Meteoritics* **20,** 175–195.

Russell S. (1992) *A Carbon and Nitrogen Isotope Study of Chondritic Diamond and Silicon Carbide*. Ph.D. dissertation, The Open University.

Russell S. S., Huss G. R., Fahey A. J., Greenwood R. C., Hutchison R., and Wasserburg G. J. (1998) An isotopic and petrologic study of calcium-aluminum-rich inclusions from CO3 meteorites. *Geochim. Cosmochim. Acta* **62,** 689–714.

Scott E. R. D. and Jones R. H. (1990) Disentangling nebular and asteroidal features of CO3 carbonaceous chondrites. *Geochim. Cosmochim. Acta* **54,** 2485–2502.

Scott E. R. D., Taylor G. J., Maggiore P., Keil K., and McKinley S. G. (1981) Three CO3 chondrites from Antarctica—Comparison of carbonaceous and ordinary type 3 chondrites. *Meteoritics* **16,** 385.

Sears D. W. G., Hasan F. A., Batchelor J. D., and Lu J. (1991a) Chemical and physical studies of type 3 chondrites—XI: Metamorphism, pairing, and brecciation of ordinary chondrites. *Proc. Lunar Planet. Sci. Conf.* **21,** 493–512.

Sears D. W. G., Batchelor J. D., Lu J., and Keck B. D. (1991b) Metamorphism of CO and CO-like chondrites and comparisons with other type 3 ordinary chondrites. *Proc. NIPR Symp. Antarct. Meteorit.* **4,** 319–343.

Simon S. B., Grossman L., Casanova I., Symes S., Benoit P., Sears D. W. G., and Wacker J. F. (1995) Axtell, a new CV3 chondrite find from Texas. *Meteoritics* **30,** 42–46.

Srinivasan G., Huss G. R., and Wasserburg G. J. (2000) A petrographic, chemical, and isotopic study of calcium-aluminum-rich inclusions and aluminum-rich chondrules from the Axtell (CV3) chondrite. *Meteorit. Planet. Sci.* **35,** 1333–1354.

Tang M. and Anders E. (1988) Isotopic anomalies of Ne, Xe, and C in meteorites. II. Interstellar diamond and SiC: Carriers of exotic noble gases. *Geochim. Cosmochim. Acta* **52,** 1235–1244.

Wasson J. T. (1985) *Meteorites*. W. H. Freeman, New York.

Weisberg M. K., Prinz M., Clayton R. N., and Mayeda T. (1993) The CR (Renazzo-type) carbonaceous chondrite group and its implications. *Geochim. Cosmochim. Acta* **57,** 1567–1586.

Wieler R., Anders E., Baur H., Lewis R. S., and Signer P. (1992) Characteristics of Q-gases and other noble gas components in the Murchison meteorite. *Geochim. Cosmochim. Acta* **56,** 2907–2921.

Wolf R., Richter G. R., Woodrow A. B., and Anders E. (1980) Chemical fractionations in meteorites—XI. C2 chondrites. *Geochim. Cosmochim. Acta* **44,** 711–717.

Yang J. and Epstein S. (1983) Interstellar organic matter in meteorites. *Geochim. Cosmochim. Acta* **47,** 2199–2216.

Yu Y., Hewins R., and Zanda B. (1996) Sodium and sulfur in chondrules: Heating time and cooling curves. In *Chondrules and the Protoplanetary Disk* (eds. R. H. Hewins, R. H. Jones, and E. R. D. Scott), pp. 213–291. Cambridge University Press, Cambridge, UK.

Zinner E., Amari S., Wopenka B., and Lewis R. S. (1995) Interstellar graphite in meteorites: Isotopic compositions and structural properties of single graphite grains from Murchison. *Meteoritics* **30,** 209–226.

Zolensky M. E. (1991) Mineralogy and matrix composition of "CR" chondrites Renazzo and EET 87770, and ungrouped chondrites Essebi and Mac87300. *Meteoritics* **26,** 414.

Appendix 1. Neon and Xenon in Acid Residues for Carbonaceous Chondrites (Xe isotopic ratios × 100)

Temp °C	^{22}Ne 10^{-8} cc/g	^{20}Ne/^{22}Ne	^{21}Ne/^{22}Ne	^{132}Xe 10^{-8} cc/g	^{124}Xe/^{132}Xe	^{126}Xe/^{132}Xe	^{128}Xe/^{132}Xe	^{129}Xe/^{132}Xe	^{130}Xe/^{132}Xe	^{131}Xe/^{132}Xe	^{134}Xe/^{132}Xe	^{136}Xe/^{132}Xe
Murchison CM2 HF-HCl Residue (AC) 162.3 ± 0.4 μg												
200				0.111	0.318 ± 0.051	0.316 ± 0.040	7.40 ± 0.16	97.8 ± 1.0	14.97 ± 0.25	77.57 ± 1.65	38.44 ± 0.58	33.07 ± 0.60
350	0.146	11.619 ± 0.961	0.0260 ± 0.0104	1.00	0.412 ± 0.011	0.371 ± 0.011	7.76 ± 0.04	101.9 ± 0.3	15.77 ± 0.08	81.14 ± 0.25	38.47 ± 0.15	32.41 ± 0.12
625	4.96	6.874 ± 0.082	0.0220 ± 0.0005	6.21	0.468 ± 0.005	0.404 ± 0.006	8.22 ± 0.03	104.1 ± 0.3	16.24 ± 0.05	81.88 ± 0.25	37.84 ± 0.10	31.69 ± 0.08
880	10.98	8.231 ± 0.041	0.0282 ± 0.0003	5.26	0.458 ± 0.008	0.408 ± 0.006	8.23 ± 0.03	103.8 ± 0.3	16.21 ± 0.05	81.99 ± 0.25	38.09 ± 0.10	31.99 ± 0.08
1100	26.48	6.397 ± 0.032	0.0231 ± 0.0002	9.24	0.462 ± 0.005	0.419 ± 0.004	8.30 ± 0.03	103.6 ± 0.3	16.33 ± 0.05	81.89 ± 0.25	38.30 ± 0.10	32.30 ± 0.08
1300	13.96	7.947 ± 0.040	0.0327 ± 0.0003	8.01	0.468 ± 0.005	0.419 ± 0.006	8.26 ± 0.03	103.7 ± 0.3	16.32 ± 0.05	82.04 ± 0.25	38.52 ± 0.10	32.54 ± 0.08
1495	8.25	8.184 ± 0.044	0.0357 ± 0.0004	5.08	0.481 ± 0.006	0.423 ± 0.006	8.35 ± 0.03	104.0 ± 0.3	16.26 ± 0.05	82.20 ± 0.25	38.97 ± 0.10	33.32 ± 0.08
1690	0.701	5.619 ± 0.376	0.0230 ± 0.0025	1.94	0.471 ± 0.008	0.423 ± 0.009	8.27 ± 0.05	103.8 ± 0.3	16.25 ± 0.06	81.97 ± 0.25	38.76 ± 0.14	32.76 ± 0.11
1769	0.958	9.424 ± 0.163	0.0323 ± 0.0024	3.69	0.466 ± 0.007	0.418 ± 0.006	8.37 ± 0.04	103.9 ± 0.3	16.30 ± 0.05	82.19 ± 0.25	38.41 ± 0.10	32.41 ± 0.08
Total	66.25	7.325 ± 0.037	0.0276 ± 0.0003	40.54	0.465 ± 0.002	0.415 ± 0.002	8.27 ± 0.02	103.7 ± 0.3	16.27 ± 0.05	81.97 ± 0.25	38.37 ± 0.10	32.38 ± 0.08
Murchison CM2 Etched HF-HCl Residue (AD) 1,746 ± 0.9 μg												
200	(0.003)			0.004	0.384 ± 0.098	0.310 ± 0.083	7.33 ± 0.34	97.9 ± 1.6	15.41 ± 0.51	79.52 ± 3.33	38.13 ± 1.02	33.02 ± 1.01
350	0.141	8.320 ± 0.128	0.0402 ± 0.0016	0.645	0.366 ± 0.004	0.337 ± 0.005	7.26 ± 0.03	98.9 ± 0.3	15.25 ± 0.05	79.14 ± 0.24	38.70 ± 0.10	32.77 ± 0.08
625	6.55	5.463 ± 0.027	0.0186 ± 0.0002	3.10	0.423 ± 0.004	0.376 ± 0.004	7.79 ± 0.02	104.0 ± 0.3	15.78 ± 0.05	81.05 ± 0.24	37.91 ± 0.10	31.58 ± 0.08
880	16.25	6.764 ± 0.034	0.0230 ± 0.0002	1.58	0.461 ± 0.005	0.410 ± 0.004	8.10 ± 0.02	104.5 ± 0.3	16.00 ± 0.05	82.36 ± 0.25	37.93 ± 0.10	31.55 ± 0.08
990	15.96	8.524 ± 0.043	0.0304 ± 0.0003	0.455	0.541 ± 0.007	0.441 ± 0.006	8.32 ± 0.03	103.7 ± 0.3	16.12 ± 0.05	82.57 ± 0.25	43.18 ± 0.11	39.45 ± 0.11
1120	37.51	7.404 ± 0.037	0.0296 ± 0.0003	0.589	0.652 ± 0.007	0.481 ± 0.005	8.83 ± 0.03	102.2 ± 0.3	16.27 ± 0.05	82.04 ± 0.24	51.12 ± 0.13	51.57 ± 0.09
1250	19.69	6.013 ± 0.030	0.0262 ± 0.0003	0.332	0.681 ± 0.010	0.499 ± 0.007	9.03 ± 0.05	102.8 ± 0.3	16.54 ± 0.06	82.16 ± 0.25	52.77 ± 0.13	54.40 ± 0.15
1395	22.01	5.882 ± 0.029	0.0265 ± 0.0003	0.488	0.676 ± 0.008	0.514 ± 0.007	9.00 ± 0.04	104.1 ± 0.3	16.41 ± 0.05	82.60 ± 0.25	52.16 ± 0.13	53.97 ± 0.12
1545	9.84	4.774 ± 0.024	0.0223 ± 0.0002	0.300	0.644 ± 0.008	0.488 ± 0.006	9.04 ± 0.04	103.0 ± 0.3	16.70 ± 0.05	81.92 ± 0.24	49.44 ± 0.12	50.50 ± 0.10
1690	2.15	3.839 ± 0.043	0.0178 ± 0.0002	0.180	0.576 ± 0.013	0.465 ± 0.009	8.84 ± 0.06	102.1 ± 0.3	16.78 ± 0.06	81.13 ± 0.25	46.15 ± 0.13	45.47 ± 0.14
1769	0.134	5.299 ± 0.261	0.0222 ± 0.0015	0.026	0.600 ± 0.032	0.416 ± 0.023	8.88 ± 0.09	103.0 ± 0.7	16.53 ± 0.18	83.18 ± 0.51	48.42 ± 0.37	48.11 ± 0.44
Total	130.23	6.638 ± 0.033	0.0265 ± 0.0003	7.69	0.490 ± 0.002	0.412 ± 0.002	8.13 ± 0.02	103.4 ± 0.3	15.97 ± 0.05	81.51 ± 0.24	41.53 ± 0.10	37.19 ± 0.09
Murchison CM2 Diamond Separate (AF) 127.7 ± 0.8 μg												
200	*0.172*	9.526 ± 0.744	0.0489 ± 0.0105	(0.006)								
350	3.61	8.716 ± 0.064	0.0288 ± 0.0007	0.501	0.493 ± 0.018	0.438 ± 0.018	8.12 ± 0.07	108.5 ± 0.7	16.23 ± 0.11	81.86 ± 0.55	38.76 ± 0.26	32.00 ± 0.19
625	82.15	8.785 ± 0.044	0.0285 ± 0.0003	21.65	0.462 ± 0.004	0.407 ± 0.004	8.07 ± 0.02	106.7 ± 0.3	15.93 ± 0.05	82.53 ± 0.25	37.91 ± 0.09	31.46 ± 0.08
780	75.85	8.596 ± 0.043	0.0291 ± 0.0003	9.29	0.472 ± 0.005	0.405 ± 0.006	8.04 ± 0.03	104.1 ± 0.3	15.88 ± 0.05	82.46 ± 0.25	38.52 ± 0.10	32.37 ± 0.08
940	80.70	8.480 ± 0.042	0.0308 ± 0.0003	2.49	0.516 ± 0.012	0.432 ± 0.009	8.17 ± 0.04	103.8 ± 0.3	15.88 ± 0.06	83.18 ± 0.23	42.02 ± 0.12	37.52 ± 0.11
1100	101.5	8.440 ± 0.042	0.0322 ± 0.0003	1.20	0.640 ± 0.013	0.494 ± 0.009	8.49 ± 0.07	102.3 ± 0.4	15.67 ± 0.07	82.99 ± 0.29	52.26 ± 0.22	53.38 ± 0.25
1300	260.5	8.471 ± 0.042	0.0338 ± 0.0003	3.68	0.760 ± 0.011	0.541 ± 0.009	8.78 ± 0.04	103.4 ± 0.3	15.59 ± 0.05	83.55 ± 0.25	60.02 ± 0.15	63.63 ± 0.16
1495	453.3	8.385 ± 0.042	0.0360 ± 0.0004	6.09	0.752 ± 0.010	0.545 ± 0.008	8.87 ± 0.03	105.7 ± 0.3	15.64 ± 0.05	83.92 ± 0.25	57.48 ± 0.14	61.39 ± 0.15
1650	34.06	7.775 ± 0.039	0.0367 ± 0.0004	0.524	0.658 ± 0.025	0.538 ± 0.022	8.86 ± 0.09	106.5 ± 0.4	16.00 ± 0.14	82.59 ± 0.43	50.80 ± 0.30	52.17 ± 0.36
1769	9.53	6.897 ± 0.059	0.0269 ± 0.0004	7.57	0.715 ± 0.008	0.529 ± 0.006	8.90 ± 0.03	105.5 ± 0.3	15.84 ± 0.05	83.32 ± 0.25	54.74 ± 0.14	57.97 ± 0.14
Total	1087.99	8.534 ± 0.043	0.0340 ± 0.0003	53.00	0.563 ± 0.003	0.454 ± 0.002	8.35 ± 0.03	105.5 ± 0.3	15.85 ± 0.05	82.89 ± 0.25	44.86 ± 0.11	42.07 ± 0.11
Murray CM2 HF-HCl Residue (AC) 226.3 ± 1.0 μg												
200	*0.066*	11.828 ± 1.171	0.0345 ± 0.0129	0.009	0.457 ± 0.237	0.240 ± 0.211	7.24 ± 0.97	97.5 ± 4.3	15.28 ± 0.77	82.13 ± 8.19	36.93 ± 2.39	33.04 ± 2.53
350	0.213	9.674 ± 0.400	0.0230 ± 0.0052	0.744	0.397 ± 0.013	0.345 ± 0.010	7.44 ± 0.05	100.2 ± 0.3	15.55 ± 0.09	80.18 ± 0.28	38.74 ± 0.19	32.71 ± 0.12
625	3.86	8.437 ± 0.046	0.0296 ± 0.0004	5.22	0.456 ± 0.005	0.410 ± 0.006	8.27 ± 0.03	104.4 ± 0.3	16.23 ± 0.05	82.05 ± 0.25	38.17 ± 0.10	31.74 ± 0.08
880	8.87	8.620 ± 0.043	0.0307 ± 0.0004	5.15	0.465 ± 0.006	0.418 ± 0.005	8.23 ± 0.03	103.8 ± 0.3	16.19 ± 0.05	81.98 ± 0.25	37.94 ± 0.10	31.78 ± 0.08
1100	26.21	7.245 ± 0.036	0.0261 ± 0.0003	8.32	0.473 ± 0.005	0.415 ± 0.005	8.31 ± 0.02	103.8 ± 0.3	16.30 ± 0.05	82.19 ± 0.25	38.24 ± 0.10	32.33 ± 0.08
1300	23.34	8.299 ± 0.041	0.0354 ± 0.0004	12.02	0.476 ± 0.004	0.418 ± 0.004	8.27 ± 0.02	103.8 ± 0.3	16.22 ± 0.05	82.16 ± 0.25	38.54 ± 0.10	32.64 ± 0.08
1495	3.72	8.221 ± 0.056	0.0413 ± 0.0007	2.75	0.478 ± 0.007	0.417 ± 0.008	8.32 ± 0.03	104.0 ± 0.3	16.20 ± 0.05	82.11 ± 0.25	39.06 ± 0.10	33.30 ± 0.08
1769	2.34	9.254 ± 0.060	0.0346 ± 0.0008	4.89	0.470 ± 0.005	0.413 ± 0.005	8.27 ± 0.03	104.1 ± 0.3	16.31 ± 0.05	82.01 ± 0.25	38.35 ± 0.10	32.41 ± 0.08
Total	68.61	8.003 ± 0.040	0.0312 ± 0.0003	39.11	0.469 ± 0.002	0.414 ± 0.002	8.26 ± 0.02	103.8 ± 0.3	16.23 ± 0.05	82.07 ± 0.25	38.37 ± 0.10	32.36 ± 0.08

(Continued)

Appendix 1. (Continued)

Temp °C	^{22}Ne 10^{-8} cc/g	$\frac{^{20}Ne}{^{22}Ne}$	$\frac{^{21}Ne}{^{22}Ne}$	^{132}Xe 10^{-8} cc/g	$\frac{^{124}Xe}{^{132}Xe}$	$\frac{^{126}Xe}{^{132}Xe}$	$\frac{^{128}Xe}{^{132}Xe}$	$\frac{^{129}Xe}{^{132}Xe}$	$\frac{^{130}Xe}{^{132}Xe}$	$\frac{^{131}Xe}{^{132}Xe}$	$\frac{^{134}Xe}{^{132}Xe}$	$\frac{^{136}Xe}{^{132}Xe}$
Murray CM2 Etched HF-HCl Residue (AD) 1,296.3 ± 1.2 μg												
200	(0.004)			0.001								
350	0.065	9.395 ± 0.217	0.0579 ± 0.0038	0.303	0.372 ± 0.006	0.336 ± 0.006	7.15 ± 0.04	98.6 ± 0.2	15.29 ± 0.05	79.09 ± 0.24	38.84 ± 0.12	33.07 ± 0.11
625	5.84	6.138 ± 0.031	0.0227 ± 0.0002	2.88	0.417 ± 0.004	0.378 ± 0.004	7.75 ± 0.02	103.3 ± 0.3	15.68 ± 0.05	80.83 ± 0.24	38.06 ± 0.10	31.73 ± 0.08
750	9.75	4.033 ± 0.020	0.0147 ± 0.0001	0.936	0.454 ± 0.006	0.405 ± 0.004	8.11 ± 0.02	105.0 ± 0.3	16.01 ± 0.05	82.40 ± 0.25	37.62 ± 0.09	31.19 ± 0.08
880	8.92	7.343 ± 0.037	0.0281 ± 0.0003	0.584	0.468 ± 0.006	0.411 ± 0.006	8.13 ± 0.03	104.6 ± 0.3	16.00 ± 0.05	82.55 ± 0.25	38.06 ± 0.09	31.91 ± 0.08
990	12.20	8.952 ± 0.045	0.0321 ± 0.0003	0.372	0.500 ± 0.007	0.428 ± 0.007	8.26 ± 0.04	104.1 ± 0.3	16.02 ± 0.05	82.68 ± 0.25	41.24 ± 0.13	36.53 ± 0.12
1120	25.24	8.292 ± 0.041	0.0329 ± 0.0003	0.418	0.593 ± 0.008	0.456 ± 0.007	8.57 ± 0.04	102.8 ± 0.3	16.18 ± 0.05	82.27 ± 0.25	47.77 ± 0.11	46.07 ± 0.12
1250	41.85	6.856 ± 0.034	0.0316 ± 0.0003	0.678	0.669 ± 0.007	0.495 ± 0.006	8.89 ± 0.03	102.6 ± 0.3	16.37 ± 0.05	82.03 ± 0.24	52.33 ± 0.10	54.01 ± 0.11
1395	25.18	5.317 ± 0.027	0.0260 ± 0.0003	0.508	0.680 ± 0.010	0.487 ± 0.008	9.00 ± 0.04	103.4 ± 0.3	16.36 ± 0.05	82.15 ± 0.25	51.98 ± 0.13	53.85 ± 0.11
1545	6.50	4.078 ± 0.021	0.0217 ± 0.0002	0.230	0.633 ± 0.008	0.481 ± 0.008	9.14 ± 0.04	103.3 ± 0.3	16.95 ± 0.08	82.33 ± 0.30	48.95 ± 0.20	49.72 ± 0.17
1595	0.951	3.706 ± 0.123	0.0218 ± 0.0005	0.093	0.587 ± 0.013	0.472 ± 0.016	9.11 ± 0.08	101.4 ± 0.4	17.15 ± 0.15	80.91 ± 0.49	45.49 ± 0.23	44.83 ± 0.22
1769	0.072	6.607 ± 0.401	0.0399 ± 0.0040	0.021	0.579 ± 0.040	0.451 ± 0.024	8.73 ± 0.20	101.9 ± 0.9	17.18 ± 0.55	85.59 ± 1.85	47.06 ± 0.54	46.03 ± 0.64
Total	136.57	6.672 ± 0.033	0.0285 ± 0.0003	7.02	0.492 ± 0.002	0.414 ± 0.002	8.15 ± 0.02	103.4 ± 0.3	15.96 ± 0.05	81.57 ± 0.24	41.65 ± 0.10	37.40 ± 0.09
Murray CM2 Diamond Separate (AF) 60.0 ± 1.0 μg												
250	(0.002)			(0.003)								
350	0.558	8.645 ± 0.503	0.0241 ± 0.0067	0.075	0.476 ± 0.142	0.239 ± 0.111	8.08 ± 0.49	104.7 ± 2.1	16.14 ± 0.41	83.62 ± 4.30	39.32 ± 1.50	30.91 ± 1.52
445	8.47	8.927 ± 0.068	0.0298 ± 0.0006	1.68	0.476 ± 0.010	0.398 ± 0.015	8.26 ± 0.08	107.7 ± 0.4	16.09 ± 0.10	82.42 ± 0.41	37.68 ± 0.26	31.71 ± 0.23
625	48.02	8.836 ± 0.044	0.0290 ± 0.0003	13.98	0.470 ± 0.007	0.417 ± 0.006	8.11 ± 0.03	107.1 ± 0.3	16.00 ± 0.05	82.70 ± 0.25	38.04 ± 0.10	31.58 ± 0.08
880	141.4	8.657 ± 0.043	0.0302 ± 0.0003	16.89	0.473 ± 0.005	0.412 ± 0.006	8.07 ± 0.03	104.7 ± 0.3	15.83 ± 0.05	82.45 ± 0.25	38.59 ± 0.10	32.38 ± 0.08
1100	242.0	8.529 ± 0.043	0.0327 ± 0.0003	3.14	0.690 ± 0.011	0.486 ± 0.012	8.54 ± 0.05	103.3 ± 0.3	15.71 ± 0.07	83.56 ± 0.36	53.16 ± 0.23	53.76 ± 0.22
1300	601.9	8.459 ± 0.042	0.0355 ± 0.0004	12.71	0.765 ± 0.009	0.536 ± 0.007	8.91 ± 0.03	105.7 ± 0.3	15.63 ± 0.05	84.06 ± 0.25	57.97 ± 0.14	61.82 ± 0.15
1495	67.09	7.861 ± 0.039	0.0365 ± 0.0004	6.62	0.689 ± 0.009	0.506 ± 0.007	8.89 ± 0.05	105.0 ± 0.3	15.96 ± 0.07	82.96 ± 0.25	52.22 ± 0.16	54.28 ± 0.15
1769	0.712	10.299 ± 0.707	0.0271 ± 0.0071	0.115	0.637 ± 0.105	0.531 ± 0.108	8.88 ± 0.47	107.2 ± 3.1	16.60 ± 0.82	84.49 ± 2.50	52.90 ± 3.12	58.98 ± 4.24
Total	1110.14	8.488 ± 0.042	0.0340 ± 0.0003	55.20	0.578 ± 0.003	0.457 ± 0.002	8.41 ± 0.03	105.6 ± 0.3	15.85 ± 0.05	83.01 ± 0.25	45.38 ± 0.11	42.83 ± 0.11
Renazzo CR2 HF-HCl Residue (AC) 149 ± 2 μg												
275	0.185	9.890 ± 0.513	0.0239 ± 0.0072									
400	0.208	9.228 ± 0.452	0.1157 ± 0.0102	0.716	0.435 ± 0.017	0.376 ± 0.019	7.93 ± 0.15	108.4 ± 0.4	15.82 ± 0.13	81.17 ± 0.41	38.52 ± 0.18	32.04 ± 0.13
500	0.395	9.733 ± 0.273	0.1129 ± 0.0062	1.20	0.437 ± 0.011	0.392 ± 0.012	8.10 ± 0.10	111.9 ± 0.3	15.89 ± 0.08	80.75 ± 0.38	38.63 ± 0.17	31.88 ± 0.09
800	0.207	9.141 ± 0.492	0.1970 ± 0.0146	0.948	0.436 ± 0.012	0.406 ± 0.013	8.12 ± 0.12	116.9 ± 0.4	15.94 ± 0.11	81.75 ± 0.36	38.26 ± 0.16	31.93 ± 0.16
915	0.388	9.153 ± 0.282	0.1162 ± 0.0063	0.462	0.452 ± 0.013	0.404 ± 0.016	7.91 ± 0.21	116.7 ± 0.6	15.99 ± 0.15	80.48 ± 0.50	37.86 ± 0.24	31.61 ± 0.22
1010	3.79	8.809 ± 0.044	0.0448 ± 0.0009	1.93	0.467 ± 0.012	0.401 ± 0.009	8.50 ± 0.07	109.8 ± 0.3	16.24 ± 0.05	82.05 ± 0.25	38.65 ± 0.11	32.86 ± 0.08
1200	15.62	8.719 ± 0.044	0.0382 ± 0.0004	7.47	0.465 ± 0.004	0.413 ± 0.005	8.27 ± 0.02	104.7 ± 0.3	16.20 ± 0.05	82.14 ± 0.25	38.51 ± 0.10	32.52 ± 0.08
1300	12.23	8.515 ± 0.043	0.0415 ± 0.0004	6.84	0.474 ± 0.005	0.413 ± 0.006	8.22 ± 0.02	104.0 ± 0.3	16.18 ± 0.05	82.09 ± 0.25	38.50 ± 0.10	32.65 ± 0.08
1490	5.55	8.237 ± 0.041	0.0447 ± 0.0008	2.86	0.492 ± 0.010	0.426 ± 0.007	8.35 ± 0.05	104.1 ± 0.3	16.11 ± 0.06	82.14 ± 0.25	39.14 ± 0.13	33.48 ± 0.09
1680	3.17	8.188 ± 0.046	0.0426 ± 0.0009	2.42	0.492 ± 0.008	0.420 ± 0.008	8.41 ± 0.05	104.1 ± 0.3	16.11 ± 0.06	82.21 ± 0.25	40.34 ± 0.13	35.22 ± 0.09
1769	1.59	9.415 ± 0.082	0.0694 ± 0.0017	0.390	0.495 ± 0.020	0.436 ± 0.019	8.90 ± 0.25	103.8 ± 0.6	16.21 ± 0.12	81.48 ± 0.49	39.97 ± 0.29	33.98 ± 0.18
1800				0.116	0.511 ± 0.045	0.448 ± 0.030	9.02 ± 0.80	102.9 ± 0.7	15.69 ± 0.35	81.16 ± 1.41	38.87 ± 0.64	34.49 ± 0.59
Total	43.33	8.617 ± 0.043	0.0444 ± 0.0004	25.36	0.471 ± 0.003	0.412 ± 0.003	8.28 ± 0.02	105.9 ± 0.3	16.14 ± 0.05	81.98 ± 0.25	38.77 ± 0.10	32.90 ± 0.08
Renazzo CR2 Etched HF-HCl Residue (AD) 747.8 ± 1.8 μg												
350	0.148	9.74 ± 2.33	0.0484 ± 0.0098	0.034	0.362 ± 0.031	0.295 ± 0.060	7.04 ± 0.22	99.0 ± 0.8	14.93 ± 0.17	78.45 ± 0.71	38.96 ± 0.39	32.65 ± 0.84
625	0.244	8.73 ± 1.57	0.146 ± 0.014	0.437	0.368 ± 0.007	0.341 ± 0.010	7.36 ± 0.05	108.9 ± 0.3	15.47 ± 0.06	79.56 ± 0.24	38.91 ± 0.14	32.87 ± 0.11
800	0.245	9.00 ± 1.66	0.149 ± 0.015	0.029	0.470 ± 0.045	0.352 ± 0.077	9.41 ± 0.22	272.7 ± 4.4	16.50 ± 0.30	83.65 ± 0.86	40.17 ± 0.51	34.47 ± 0.96
960	1.85	8.724 ± 0.201	0.0670 ± 0.0014	0.057	0.532 ± 0.031	0.423 ± 0.042	9.12 ± 0.21	149.1 ± 1.1	15.92 ± 0.13	82.68 ± 0.74	45.12 ± 0.39	41.83 ± 0.50
1130	43.66	8.373 ± 0.042	0.0388 ± 0.0004	1.081	0.728 ± 0.010	0.534 ± 0.007	8.87 ± 0.04	106.6 ± 0.2	15.62 ± 0.05	83.77 ± 0.25	56.98 ± 0.14	60.55 ± 0.15
1250	9.93	7.999 ± 0.045	0.0524 ± 0.0005	0.229	0.726 ± 0.017	0.521 ± 0.014	8.93 ± 0.08	105.8 ± 0.4	15.75 ± 0.08	84.09 ± 0.45	57.14 ± 0.27	60.90 ± 0.18
1400	3.17	6.421 ± 0.111	0.1514 ± 0.0020	0.084	0.701 ± 0.033	0.548 ± 0.020	8.82 ± 0.13	105.5 ± 0.6	16.11 ± 0.12	82.05 ± 0.56	55.08 ± 0.37	58.16 ± 0.35
1620	0.524	3.923 ± 0.614	0.394 ± 0.022	0.019	0.491 ± 0.099	0.376 ± 0.080	8.99 ± 0.35	103.1 ± 1.7	16.09 ± 0.33	82.38 ± 1.07	50.13 ± 0.91	51.62 ± 0.48

(Continued)

Appendix 1. (Continued)

Temp °C	^{22}Ne 10^{-8} cc/g	^{20}Ne/^{22}Ne	^{21}Ne/^{22}Ne	^{132}Xe 10^{-8} cc/g	^{124}Xe/^{132}Xe	^{126}Xe/^{132}Xe	^{128}Xe/^{132}Xe	^{129}Xe/^{132}Xe	^{130}Xe/^{132}Xe	^{131}Xe/^{132}Xe	^{134}Xe/^{132}Xe	^{136}Xe/^{132}Xe
1769	0.045	2.62 ± 9.46	0.586 ± 0.120	0.001								
Total	59.81	8.182 ± 0.041	0.0523 ± 0.0005	1.971	0.629 ± 0.007	0.479 ± 0.005	8.53 ± 0.03	110.4 ± 0.3	15.64 ± 0.05	82.66 ± 0.25	51.95 ± 0.13	52.86 ± 0.13
Renazzo CR2 Diamond Separate (AF) 101.7 ± 1.5 μg												
350	0.280	10.90 ± 0.77	0.0521 ± 0.0079	0.010	0.042 ± 0.524	0.027 ± 0.406	7.10 ± 1.52	115.2 ± 7.7	13.12 ± 1.73	77.2 ± 14.8	39.29 ± 3.73	40.40 ± 3.06
625	31.5	8.521 ± 0.043	0.0323 ± 0.0003	0.655	0.610 ± 0.022	0.464 ± 0.025	9.15 ± 0.07	234.3 ± 1.9	15.51 ± 0.14	82.18 ± 0.47	49.74 ± 0.33	49.17 ± 0.27
880	83.0	8.564 ± 0.043	0.0317 ± 0.0003	1.45	0.618 ± 0.015	0.443 ± 0.012	8.88 ± 0.08	159.9 ± 0.6	15.84 ± 0.11	83.55 ± 0.39	48.56 ± 0.19	46.96 ± 0.20
1100	206.1	8.488 ± 0.042	0.0336 ± 0.0003	2.15	0.749 ± 0.014	0.527 ± 0.010	9.01 ± 0.05	105.1 ± 0.3	15.57 ± 0.09	83.72 ± 0.28	59.54 ± 0.20	63.17 ± 0.19
1300	422.6	8.453 ± 0.042	0.0355 ± 0.0004	6.87	0.797 ± 0.008	0.563 ± 0.008	8.97 ± 0.04	105.0 ± 0.3	15.55 ± 0.05	83.95 ± 0.25	61.97 ± 0.15	67.32 ± 0.17
1690	297.7	8.254 ± 0.041	0.0375 ± 0.0004	6.37	0.759 ± 0.010	0.542 ± 0.008	9.05 ± 0.03	106.6 ± 0.3	15.71 ± 0.06	83.60 ± 0.25	57.29 ± 0.14	61.57 ± 0.16
1769	6.20	8.330 ± 0.073	0.0360 ± 0.0008	5.95	0.745 ± 0.008	0.544 ± 0.009	8.99 ± 0.04	106.5 ± 0.3	15.63 ± 0.05	83.62 ± 0.25	57.14 ± 0.14	61.71 ± 0.17
Total	1047.30	8.414 ± 0.042	0.0353 ± 0.0004	23.46	0.752 ± 0.004	0.539 ± 0.004	9.00 ± 0.03	112.9 ± 0.3	15.63 ± 0.05	83.67 ± 0.25	58.07 ± 0.15	62.17 ± 0.16
ALHA77307 CO3 HF-HCl Residue (AC) 39.1 ± 7.4 μg												
350	(0.028)			0.230	0.108 ± 0.075	0.138 ± 0.073	6.81 ± 0.27	97.8 ± 1.2	14.91 ± 0.39	77.32 ± 0.91	38.68 ± 0.68	33.09 ± 0.77
575	0.780	10.7 ± 14.3	0.099 ± 0.079	9.79	0.381 ± 0.006	0.351 ± 0.003	7.38 ± 0.04	101.1 ± 0.3	15.37 ± 0.05	79.47 ± 0.24	38.77 ± 0.10	32.80 ± 0.08
800	0.833	10.4 ± 13.7	0.166 ± 0.093	1.64	0.461 ± 0.017	0.408 ± 0.016	8.20 ± 0.06	113.5 ± 0.5	16.21 ± 0.18	81.23 ± 0.50	38.12 ± 0.30	32.09 ± 0.29
1000	6.85	8.8 ± 1.5	0.093 ± 0.010	4.39	0.493 ± 0.010	0.441 ± 0.008	8.26 ± 0.05	103.7 ± 0.3	16.26 ± 0.08	81.90 ± 0.36	38.23 ± 0.15	32.23 ± 0.16
1200	9.98	8.7 ± 1.0	0.0795 ± 0.0069	7.23	0.472 ± 0.008	0.417 ± 0.005	8.24 ± 0.03	104.0 ± 0.3	16.27 ± 0.08	82.20 ± 0.25	38.53 ± 0.10	32.33 ± 0.09
1425	8.49	7.2 ± 1.2	0.106 ± 0.010	3.66	0.469 ± 0.011	0.410 ± 0.010	8.31 ± 0.05	103.8 ± 0.3	16.27 ± 0.07	82.17 ± 0.33	38.76 ± 0.19	32.78 ± 0.15
1650	4.57	7.8 ± 2.3	0.111 ± 0.019	1.89	0.489 ± 0.019	0.409 ± 0.016	8.40 ± 0.09	104.0 ± 0.4	15.99 ± 0.15	81.60 ± 0.41	39.61 ± 0.23	34.36 ± 0.32
1769	2.15	8.86 ± 5.58	0.109 ± 0.040	1.59	0.525 ± 0.021	0.426 ± 0.017	8.31 ± 0.09	103.1 ± 0.4	16.21 ± 0.17	81.23 ± 0.47	39.06 ± 0.28	33.97 ± 0.32
Total	33.65	8.31 ± 0.86	0.0975 ± 0.0061	30.42	0.446 ± 0.004	0.396 ± 0.003	7.98 ± 0.02	103.4 ± 0.3	15.94 ± 0.05	81.10 ± 0.24	38.67 ± 0.10	32.73 ± 0.08
ALHA77307 CO3 Etched HF-HCl Residue (AD) 708 ± 7 μg												
350	*0.013*		0.457 ± 0.264	1.20	0.358 ± 0.003	0.329 ± 0.004	7.14 ± 0.03	99.0 ± 0.3	15.15 ± 0.05	79.04 ± 0.24	38.76 ± 0.10	32.98 ± 0.08
575	0.430	6.75 ± 1.01	0.1978 ± 0.0134	6.43	0.353 ± 0.002	0.329 ± 0.002	7.11 ± 0.02	105.6 ± 0.3	15.07 ± 0.05	78.96 ± 0.24	38.62 ± 0.10	32.66 ± 0.08
775	1.86	8.062 ± 0.244	0.0890 ± 0.0019	0.193	0.478 ± 0.015	0.411 ± 0.012	8.13 ± 0.05	193.2 ± 1.0	16.00 ± 0.07	81.56 ± 0.27	38.30 ± 0.16	32.10 ± 0.16
950	8.92	8.257 ± 0.053	0.0579 ± 0.0006	0.342	0.542 ± 0.009	0.450 ± 0.009	8.31 ± 0.05	109.0 ± 0.3	15.93 ± 0.07	82.65 ± 0.25	43.53 ± 0.18	39.87 ± 0.13
1125	21.66	8.165 ± 0.041	0.0515 ± 0.0005	0.528	0.672 ± 0.008	0.507 ± 0.006	8.65 ± 0.04	104.5 ± 0.3	15.83 ± 0.06	82.92 ± 0.25	52.93 ± 0.13	53.78 ± 0.13
1275	13.90	6.628 ± 0.033	0.0601 ± 0.0006	0.310	0.690 ± 0.011	0.505 ± 0.010	8.87 ± 0.04	103.4 ± 0.3	16.31 ± 0.07	81.99 ± 0.28	52.85 ± 0.18	54.16 ± 0.17
1475	5.76	6.548 ± 0.073	0.0930 ± 0.0009	0.205	0.648 ± 0.016	0.497 ± 0.012	8.88 ± 0.06	103.0 ± 0.4	16.57 ± 0.09	81.31 ± 0.34	50.41 ± 0.19	51.28 ± 0.19
1700	1.42	5.589 ± 0.287	0.1576 ± 0.0044	0.092	0.566 ± 0.047	0.440 ± 0.050	9.33 ± 0.09	98.5 ± 0.3	17.90 ± 0.18	78.13 ± 0.38	44.80 ± 0.23	43.91 ± 0.36
1769	0.103	4.91 ± 4.67	0.2325 ± 0.0570	0.016	0.487 ± 0.141	0.393 ± 0.127	9.15 ± 0.23	99.9 ± 1.0	18.25 ± 0.52	78.16 ± 1.02	42.18 ± 1.17	38.04 ± 2.24
Total	54.08	7.522 ± 0.038	0.0649 ± 0.0006	9.32	0.401 ± 0.002	0.356 ± 0.002	7.39 ± 0.02	106.4 ± 0.3	15.28 ± 0.05	79.53 ± 0.24	40.42 ± 0.10	35.40 ± 0.09
ALHA77307 CO3 Diamond Separate (AF) 135.6 ± 5.3 μg												
350	0.974	8.76 ± 2.44	0.0507 ± 0.0116	0.036	0.490 ± 0.088	0.289 ± 0.097	8.09 ± 0.47	345 ± 14	16.62 ± 0.52	80.48 ± 1.87	41.96 ± 1.19	38.43 ± 2.48
600	50.05	8.660 ± 0.049	0.0349 ± 0.0003	3.37	0.489 ± 0.004	0.425 ± 0.006	8.11 ± 0.04	383.6 ± 1.2	15.99 ± 0.07	82.28 ± 0.25	39.69 ± 0.13	33.91 ± 0.08
800	66.97	8.623 ± 0.043	0.0333 ± 0.0003	4.65	0.484 ± 0.005	0.411 ± 0.004	8.12 ± 0.02	128.1 ± 0.4	15.86 ± 0.05	82.45 ± 0.25	39.43 ± 0.10	33.61 ± 0.08
920	62.07	8.522 ± 0.044	0.0340 ± 0.0003	1.38	0.561 ± 0.010	0.453 ± 0.008	8.28 ± 0.05	105.6 ± 0.3	15.82 ± 0.07	82.77 ± 0.25	44.14 ± 0.18	40.63 ± 0.14
1100	110.8	8.494 ± 0.042	0.0350 ± 0.0004	1.16	0.687 ± 0.009	0.486 ± 0.008	8.56 ± 0.05	102.9 ± 0.3	15.62 ± 0.08	82.57 ± 0.25	55.99 ± 0.18	57.35 ± 0.17
1225	125.4	8.506 ± 0.043	0.0369 ± 0.0004	1.53	0.765 ± 0.011	0.531 ± 0.008	8.75 ± 0.05	103.2 ± 0.3	15.46 ± 0.09	83.43 ± 0.25	60.33 ± 0.23	64.15 ± 0.21
1375	195.9	8.486 ± 0.042	0.0381 ± 0.0004	3.91	0.769 ± 0.006	0.532 ± 0.005	8.78 ± 0.03	104.2 ± 0.3	15.51 ± 0.05	83.83 ± 0.25	60.10 ± 0.15	64.12 ± 0.16
1525	257.4	8.385 ± 0.042	0.0397 ± 0.0004	8.03	0.738 ± 0.004	0.533 ± 0.003	8.81 ± 0.03	105.7 ± 0.3	15.58 ± 0.05	83.84 ± 0.25	56.98 ± 0.14	60.50 ± 0.15
1700	57.57	8.044 ± 0.043	0.0425 ± 0.0004	3.11	0.673 ± 0.005	0.512 ± 0.004	8.79 ± 0.03	106.2 ± 0.3	15.87 ± 0.05	83.01 ± 0.25	51.61 ± 0.13	53.85 ± 0.14
1769	7.08	7.968 ± 0.349	0.0432 ± 0.0017	1.87	0.706 ± 0.011	0.501 ± 0.007	8.81 ± 0.04	105.4 ± 0.3	15.78 ± 0.06	83.31 ± 0.25	53.43 ± 0.17	55.79 ± 0.19
1800	0.159		0.159 ± 0.128	0.468	0.673 ± 0.017	0.508 ± 0.016	8.88 ± 0.10	104.6 ± 0.3	15.95 ± 0.14	82.72 ± 0.55	52.91 ± 0.28	54.96 ± 0.34
Total	934.2	8.453 ± 0.042	0.0375 ± 0.0004	29.50	0.655 ± 0.003	0.491 ± 0.002	8.58 ± 0.03	140.9 ± 0.4	15.72 ± 0.05	83.18 ± 0.25	51.31 ± 0.13	51.72 ± 0.13
Colony CO3 HF-HCl Residue (AC) 186 ± 2 μg												
200	(0.029)											
350	0.268	11.67 ± 5.66	0.0905 ± 0.0264	0.097	0.437 ± 0.042	0.423 ± 0.042	8.00 ± 0.14	104.0 ± 0.7	16.26 ± 0.20	80.69 ± 0.81	38.68 ± 0.40	33.35 ± 0.46
625	0.770	9.54 ± 1.85	0.1682 ± 0.0175	0.683	0.456 ± 0.017	0.424 ± 0.013	8.17 ± 0.07	106.1 ± 0.4	16.22 ± 0.08	81.62 ± 0.37	38.06 ± 0.23	31.76 ± 0.20

(Continued)

Appendix 1. continued

Temp °C	^{22}Ne 10^{-8} cc/g	^{20}Ne/^{22}Ne	^{21}Ne/^{22}Ne	^{132}Xe 10^{-8} cc/g	^{124}Xe/^{132}Xe	^{126}Xe/^{132}Xe	^{128}Xe/^{132}Xe	^{129}Xe/^{132}Xe	^{130}Xe/^{132}Xe	^{131}*Xe*/^{132}*Xe*	^{134}Xe/^{132}Xe	^{136}Xe/^{132}Xe
850	3.72	8.373 ± 0.385	0.1152 ± 0.0041	0.983	0.464 ± 0.016	0.408 ± 0.012	8.41 ± 0.07	106.2 ± 0.4	16.32 ± 0.10	82.34 ± 0.26	38.82 ± 0.20	32.66 ± 0.12
1100	10.70	8.105 ± 0.134	0.0911 ± 0.0014	2.31	0.476 ± 0.008	0.420 ± 0.008	8.37 ± 0.04	103.9 ± 0.3	16.33 ± 0.05	82.37 ± 0.25	39.46 ± 0.11	33.84 ± 0.10
1300	5.52	5.266 ± 0.186	0.2507 ± 0.0044	0.973	0.473 ± 0.015	0.418 ± 0.015	8.37 ± 0.07	102.8 ± 0.3	16.27 ± 0.09	82.16 ± 0.38	39.39 ± 0.18	34.01 ± 0.18
1450	1.30	4.855 ± 0.815	0.4108 ± 0.0227	0.259	0.440 ± 0.035	0.398 ± 0.033	8.27 ± 0.12	104.1 ± 0.8	16.21 ± 0.18	82.27 ± 0.53	39.83 ± 0.39	34.21 ± 0.33
1769	0.689	3.38 ± 1.56	0.5384 ± 0.0437	0.265	0.481 ± 0.033	0.376 ± 0.032	8.23 ± 0.12	102.9 ± 0.8	16.19 ± 0.17	81.54 ± 0.45	38.47 ± 0.32	33.66 ± 0.24
1800				*0.002*								
Total	23.00	7.230 ± 0.149	0.1674 ± 0.0024	5.57	0.469 ± 0.006	0.415 ± 0.005	8.34 ± 0.03	104.3 ± 0.3	16.29 ± 0.05	82.16 ± 0.25	39.12 ± 0.10	33.41 ± 0.08
Colony CO3 Etched HF-HCl Residue (AD) 1,112 ± 2 μg												
350	*0.014*			0.061	0.367 ± 0.038	0.309 ± 0.020	7.26 ± 0.09	98.6 ± 0.5	15.33 ± 0.13	78.93 ± 0.52	38.76 ± 0.24	32.88 ± 0.24
625	0.62	8.319 ± 0.337	0.1911 ± 0.0056	0.139	0.462 ± 0.020	0.395 ± 0.014	8.12 ± 0.06	111.8 ± 0.4	15.77 ± 0.08	80.97 ± 0.33	38.61 ± 0.14	32.55 ± 0.19
800	1.05	8.411 ± 0.194	0.1335 ± 0.0024	0.067	0.503 ± 0.037	0.403 ± 0.028	8.88 ± 0.09	148.7 ± 0.8	16.28 ± 0.11	82.21 ± 0.49	38.53 ± 0.28	32.63 ± 0.20
950	13.19	8.418 ± 0.042	0.0569 ± 0.0006	0.436	0.590 ± 0.010	0.476 ± 0.009	8.69 ± 0.03	109.1 ± 0.3	15.83 ± 0.06	83.27 ± 0.25	48.97 ± 0.14	48.23 ± 0.14
1120	19.68	8.489 ± 0.042	0.0181 ± 0.0002	0.497	0.689 ± 0.009	0.509 ± 0.010	8.85 ± 0.05	105.2 ± 0.3	15.97 ± 0.09	83.18 ± 0.25	53.51 ± 0.13	55.83 ± 0.15
1300	4.37	5.528 ± 0.047	0.1676 ± 0.0017	0.068	0.642 ± 0.026	0.495 ± 0.022	9.41 ± 0.09	99.9 ± 0.4	17.49 ± 0.14	80.08 ± 0.46	50.01 ± 0.28	51.44 ± 0.20
1450	3.58	3.923 ± 0.053	0.3504 ± 0.0035	0.061	0.615 ± 0.023	0.493 ± 0.018	9.13 ± 0.13	101.5 ± 0.6	16.97 ± 0.15	80.63 ± 0.52	47.95 ± 0.30	48.99 ± 0.38
1769	0.37	2.431 ± 0.520	0.6283 ± 0.0340	0.009	0.543 ± 0.108	0.395 ± 0.081	9.50 ± 0.24	89.7 ± 1.2	19.69 ± 0.43	73.15 ± 1.09	39.57 ± 0.87	38.09 ± 0.74
1800	0.032	10.220 ± 7.897	0.0802 ± 0.0351	0.001								
Total	42.90	7.730 ± 0.039	0.0836 ± 0.0008	1.339	0.602 ± 0.006	0.470 ± 0.005	8.70 ± 0.03	108.5 ± 0.3	16.04 ± 0.05	82.39 ± 0.25	48.53 ± 0.12	48.06 ± 0.12
Colony CO3 Diamond Separate (AF) 150.7 ± 1.0 μg												
200	0.599	9.701 ± 0.267	0.0289 ± 0.0031	*0.001*								
350	2.51	8.526 ± 0.078	0.0339 ± 0.0010	0.074	0.559 ± 0.128	0.403 ± 0.054	9.20 ± 0.20	127.2 ± 1.5	15.10 ± 0.30	82.38 ± 1.33	43.32 ± 0.84	39.51 ± 1.51
625	57.18	8.552 ± 0.043	0.0327 ± 0.0003	2.73	0.496 ± 0.011	0.409 ± 0.007	9.06 ± 0.04	142.4 ± 0.3	15.90 ± 0.05	82.33 ± 0.25	41.41 ± 0.13	36.64 ± 0.10
800	77.87	8.538 ± 0.043	0.0327 ± 0.0003	3.94	0.487 ± 0.007	0.427 ± 0.006	8.43 ± 0.03	115.5 ± 0.3	15.86 ± 0.05	82.84 ± 0.25	40.63 ± 0.11	35.35 ± 0.09
950	73.26	8.483 ± 0.042	0.0344 ± 0.0003	1.12	0.582 ± 0.016	0.470 ± 0.014	8.69 ± 0.05	105.4 ± 0.4	15.73 ± 0.07	82.52 ± 0.29	47.78 ± 0.21	46.06 ± 0.16
1110	145.6	8.440 ± 0.042	0.0349 ± 0.0003	1.41	0.724 ± 0.014	0.506 ± 0.011	8.96 ± 0.06	102.7 ± 0.3	15.39 ± 0.06	83.01 ± 0.27	58.43 ± 0.20	61.57 ± 0.18
1250	170.1	8.434 ± 0.042	0.0357 ± 0.0004	2.20	0.783 ± 0.014	0.545 ± 0.010	9.02 ± 0.04	103.3 ± 0.3	15.45 ± 0.08	83.50 ± 0.25	60.74 ± 0.15	65.42 ± 0.17
1395	321.4	8.386 ± 0.042	0.0369 ± 0.0004	7.68	0.775 ± 0.008	0.535 ± 0.006	8.97 ± 0.03	105.2 ± 0.3	15.53 ± 0.05	83.72 ± 0.25	59.55 ± 0.15	64.06 ± 0.16
1545	182.3	8.217 ± 0.041	0.0385 ± 0.0004	7.35	0.725 ± 0.008	0.531 ± 0.006	8.94 ± 0.03	106.2 ± 0.3	15.66 ± 0.05	83.40 ± 0.25	54.91 ± 0.14	58.66 ± 0.15
1690	13.03	7.826 ± 0.039	0.0423 ± 0.0005	1.29	0.705 ± 0.014	0.504 ± 0.014	8.95 ± 0.05	106.8 ± 0.3	15.87 ± 0.09	83.50 ± 0.30	51.43 ± 0.18	53.49 ± 0.22
1769	5.53	8.228 ± 0.050	0.0381 ± 0.0006	0.419	0.725 ± 0.027	0.504 ± 0.021	8.86 ± 0.12	105.4 ± 0.4	15.69 ± 0.17	83.85 ± 0.57	54.98 ± 0.34	56.94 ± 0.51
Total	1049.24	8.392 ± 0.042	0.0361 ± 0.0004	28.22	0.681 ± 0.004	0.501 ± 0.003	8.89 ± 0.03	110.4 ± 0.3	15.66 ± 0.05	83.27 ± 0.25	53.03 ± 0.13	54.61 ± 0.14
Mokoia CV3 HF-HCl Residue (AC) 301.5 ± 2.0 μg												
200	0.005											
350	0.513	10.65 ± 1.26	0.0983 ± 0.0082	0.594	0.429 ± 0.021	0.407 ± 0.016	7.77 ± 0.06	115.4 ± 0.4	15.95 ± 0.08	80.42 ± 0.30	38.26 ± 0.17	32.29 ± 0.17
550	0.452	10.80 ± 1.14	0.1026 ± 0.0075	0.545	0.464 ± 0.021	0.412 ± 0.014	8.19 ± 0.08	121.6 ± 0.4	16.15 ± 0.09	81.46 ± 0.27	37.89 ± 0.15	32.06 ± 0.15
750	0.551	10.45 ± 1.04	0.1234 ± 0.0083	0.250	0.503 ± 0.043	0.435 ± 0.027	8.12 ± 0.08	115.1 ± 0.8	16.09 ± 0.14	80.97 ± 0.47	38.27 ± 0.25	31.56 ± 0.24
950	5.25	9.054 ± 0.113	0.0506 ± 0.0007	0.582	0.501 ± 0.020	0.428 ± 0.014	8.26 ± 0.06	106.4 ± 0.5	16.25 ± 0.08	82.00 ± 0.39	39.79 ± 0.19	34.34 ± 0.17
1150	11.08	8.867 ± 0.057	0.0435 ± 0.0004	2.34	0.481 ± 0.008	0.400 ± 0.008	8.28 ± 0.03	104.0 ± 0.3	16.27 ± 0.05	82.01 ± 0.25	38.68 ± 0.10	32.97 ± 0.10
1350	24.18	8.536 ± 0.043	0.0520 ± 0.0005	5.87	0.481 ± 0.007	0.417 ± 0.005	8.24 ± 0.02	103.7 ± 0.3	16.19 ± 0.05	82.15 ± 0.25	38.88 ± 0.10	33.19 ± 0.08
1550	9.46	8.109 ± 0.058	0.0789 ± 0.0008	2.43	0.484 ± 0.007	0.424 ± 0.008	8.30 ± 0.04	103.7 ± 0.3	16.17 ± 0.05	82.00 ± 0.25	40.36 ± 0.10	35.34 ± 0.10
1750	5.85	9.051 ± 0.108	0.0645 ± 0.0008	1.33	0.530 ± 0.008	0.428 ± 0.009	8.24 ± 0.05	103.4 ± 0.3	16.02 ± 0.05	82.09 ± 0.25	41.59 ± 0.13	37.62 ± 0.12
Total	57.34	8.685 ± 0.043	0.0574 ± 0.0006	13.94	0.484 ± 0.004	0.417 ± 0.003	8.23 ± 0.02	105.2 ± 0.3	16.17 ± 0.05	81.97 ± 0.25	39.33 ± 0.10	33.89 ± 0.08
Mokoia CV3 Etched HF-HCl Residue (AD) 817 ± 2 μg												
350	0.002			0.006	0.624 ± 0.207	0.434 ± 0.198	7.64 ± 0.52	104.5 ± 2.6	15.42 ± 0.50	81.68 ± 1.95	38.13 ± 1.32	32.48 ± 2.30
625	0.44	10.667 ± 0.685	0.1209 ± 0.0059	0.056	0.436 ± 0.031	0.389 ± 0.032	7.81 ± 0.11	154.1 ± 1.1	15.86 ± 0.13	80.98 ± 0.82	38.89 ± 0.35	32.39 ± 0.39
800	Gas lost			Gas lost								
950	4.26	8.901 ± 0.062	0.0574 ± 0.0006	0.079	0.619 ± 0.037	0.500 ± 0.031	8.35 ± 0.11	131.1 ± 0.7	15.72 ± 0.15	83.78 ± 0.46	47.92 ± 0.30	46.49 ± 0.36
1120	32.55	8.468 ± 0.042	0.0418 ± 0.0004	0.657	0.720 ± 0.011	0.510 ± 0.007	8.73 ± 0.04	104.7 ± 0.3	15.56 ± 0.06	83.36 ± 0.25	56.53 ± 0.16	59.71 ± 0.15

(Continued)

Appendix 1. (Continued)

Temp °C	^{22}Ne 10^{-8} cc/g	$\frac{^{20}Ne}{^{22}Ne}$	$\frac{^{21}Ne}{^{22}Ne}$	^{132}Xe 10^{-8} cc/g	$\frac{^{124}Xe}{^{132}Xe}$	$\frac{^{126}Xe}{^{132}Xe}$	$\frac{^{128}Xe}{^{132}Xe}$	$\frac{^{129}Xe}{^{132}Xe}$	$\frac{^{130}Xe}{^{132}Xe}$	$\frac{^{131}Xe}{^{132}Xe}$	$\frac{^{134}Xe}{^{132}Xe}$	$\frac{^{136}Xe}{^{132}Xe}$
1300	18.55	8.226 ± 0.041	0.0526 ± 0.0005	0.435	0.773 ± 0.019	0.535 ± 0.012	8.80 ± 0.04	105.1 ± 0.3	15.66 ± 0.07	83.82 ± 0.25	57.65 ± 0.16	61.90 ± 0.19
1450	6.69	7.461 ± 0.040	0.1341 ± 0.0013	0.176	0.718 ± 0.017	0.511 ± 0.011	8.90 ± 0.09	106.1 ± 0.4	15.72 ± 0.10	84.36 ± 0.39	57.19 ± 0.32	61.07 ± 0.30
1610	1.26	5.248 ± 0.167	0.3580 ± 0.0072	0.066	0.666 ± 0.037	0.508 ± 0.026	8.71 ± 0.13	104.4 ± 0.7	15.76 ± 0.14	82.93 ± 0.70	53.74 ± 0.48	56.50 ± 0.38
1769	0.082	4.75 ± 2.95	0.5867 ± 0.0666	0.002	0.671 ± 0.449	0.498 ± 0.379	7.41 ± 1.25	107.9 ± 4.0	15.86 ± 1.19	77.32 ± 4.78	49.92 ± 2.87	47.25 ± 2.67
Total	63.83	8.268 ± 0.041	0.0632 ± 0.0006	1.478	0.717 ± 0.008	0.512 ± 0.005	8.71 ± 0.03	108.3 ± 0.3	15.64 ± 0.05	83.51 ± 0.25	55.59 ± 0.14	58.49 ± 0.15
Mokoia CV3 Diamond Separate (AF) 158 ± 1.0 μg												
200	0.206	9.721 ± 0.690	0.0385 ± 0.0090									
350	2.80	8.518 ± 0.084	0.0347 ± 0.0008	0.043	0.710 ± 0.205	0.488 ± 0.082	8.60 ± 0.36	138.7 ± 3.1	15.45 ± 0.43	86.46 ± 1.87	55.67 ± 1.60	55.67 ± 1.39
625	66.37	8.557 ± 0.043	0.0325 ± 0.0003	1.15	0.617 ± 0.015	0.471 ± 0.011	8.39 ± 0.06	190.7 ± 0.7	15.68 ± 0.07	82.96 ± 0.28	50.00 ± 0.20	49.50 ± 0.19
800	71.82	8.531 ± 0.043	0.0328 ± 0.0003	1.20	0.597 ± 0.012	0.475 ± 0.016	8.25 ± 0.07	118.7 ± 0.4	15.73 ± 0.09	83.27 ± 0.24	48.38 ± 0.20	46.65 ± 0.19
950	73.46	8.462 ± 0.042	0.0342 ± 0.0003	0.80	0.702 ± 0.017	0.514 ± 0.018	8.63 ± 0.09	104.2 ± 0.4	15.46 ± 0.08	82.95 ± 0.27	56.35 ± 0.26	58.36 ± 0.17
1110	127.0	8.440 ± 0.042	0.0343 ± 0.0003	1.24	0.790 ± 0.014	0.555 ± 0.011	8.89 ± 0.07	103.5 ± 0.3	15.42 ± 0.07	83.72 ± 0.29	61.27 ± 0.19	65.96 ± 0.19
1250	208.1	8.433 ± 0.042	0.0354 ± 0.0004	2.89	0.808 ± 0.012	0.542 ± 0.009	8.87 ± 0.04	104.2 ± 0.3	15.49 ± 0.07	84.06 ± 0.25	62.27 ± 0.15	67.31 ± 0.17
1395	236.7	8.390 ± 0.042	0.0365 ± 0.0004	4.80	0.780 ± 0.008	0.557 ± 0.008	8.98 ± 0.04	104.9 ± 0.3	15.53 ± 0.05	83.67 ± 0.25	61.34 ± 0.15	66.70 ± 0.17
1545	247.4	8.289 ± 0.041	0.0378 ± 0.0004	6.03	0.769 ± 0.007	0.553 ± 0.007	9.01 ± 0.04	106.8 ± 0.3	15.64 ± 0.05	84.10 ± 0.25	58.05 ± 0.15	62.88 ± 0.16
1769	36.90	8.022 ± 0.040	0.0402 ± 0.0004	5.05	0.734 ± 0.009	0.528 ± 0.006	8.96 ± 0.04	106.4 ± 0.3	15.67 ± 0.05	83.70 ± 0.25	55.79 ± 0.14	59.80 ± 0.15
Total	1070.68	8.394 ± 0.042	0.0358 ± 0.0004	23.21	0.751 ± 0.004	0.537 ± 0.003	8.88 ± 0.03	110.6 ± 0.3	15.59 ± 0.05	83.76 ± 0.25	57.97 ± 0.14	62.04 ± 0.16
Axtell CV3 HF-HCl Residue (AC) 579 ± 6 μg												
350	0.032			0.106	0.371 ± 0.015	0.330 ± 0.013	7.15 ± 0.07	100.8 ± 0.4	14.96 ± 0.14	78.93 ± 0.39	38.85 ± 0.30	32.75 ± 0.23
575	0.760	8.640 ± 0.389	0.3529 ± 0.0159	1.05	0.437 ± 0.005	0.390 ± 0.006	8.01 ± 0.03	165.1 ± 0.5	15.89 ± 0.05	81.06 ± 0.24	38.52 ± 0.10	32.50 ± 0.08
800	0.419	9.355 ± 0.804	0.4725 ± 0.0406	0.714	0.459 ± 0.004	0.402 ± 0.004	8.41 ± 0.04	242.7 ± 0.7	16.25 ± 0.05	81.88 ± 0.25	38.52 ± 0.10	32.63 ± 0.08
950	3.720	8.330 ± 0.105	0.1175 ± 0.0016	0.462	0.495 ± 0.008	0.428 ± 0.008	8.63 ± 0.04	203.0 ± 0.6	16.20 ± 0.06	82.05 ± 0.25	40.56 ± 0.10	35.92 ± 0.10
1100	14.22	8.598 ± 0.043	0.0478 ± 0.0026	0.954	0.521 ± 0.005	0.436 ± 0.003	8.39 ± 0.04	119.9 ± 0.4	16.09 ± 0.05	82.16 ± 0.25	41.59 ± 0.10	37.25 ± 0.10
1250	32.03	8.478 ± 0.042	0.0460 ± 0.0005	2.68	0.501 ± 0.003	0.427 ± 0.002	8.33 ± 0.02	107.0 ± 0.3	16.14 ± 0.05	82.28 ± 0.25	40.67 ± 0.10	35.87 ± 0.09
1400	15.38	8.416 ± 0.042	0.0613 ± 0.0006	3.38	0.495 ± 0.003	0.421 ± 0.002	8.33 ± 0.02	105.3 ± 0.3	16.17 ± 0.05	82.29 ± 0.25	40.22 ± 0.10	35.12 ± 0.09
1650	4.94	7.942 ± 0.087	0.1326 ± 0.0017	2.45	0.513 ± 0.004	0.432 ± 0.003	8.35 ± 0.03	104.8 ± 0.3	16.11 ± 0.05	82.32 ± 0.25	41.42 ± 0.10	36.98 ± 0.09
1789	0.691	11.92 ± 1.02	0.0771 ± 0.0066	1.08	0.498 ± 0.004	0.420 ± 0.004	8.32 ± 0.02	104.3 ± 0.3	16.20 ± 0.05	82.10 ± 0.25	40.48 ± 0.10	35.42 ± 0.09
Total	72.19	8.503 ± 0.043	0.0653 ± 0.0007	12.87	0.494 ± 0.002	0.421 ± 0.002	8.32 ± 0.02	122.6 ± 0.4	16.12 ± 0.05	82.11 ± 0.25	40.43 ± 0.10	35.47 ± 0.09
Axtell CV3 Etched HF-HCl Residue (AD) 570 ± 3 μg												
440	0.29	5.969 ± 0.161	0.3153 ± 0.0100	0.032	0.555 ± 0.036	0.435 ± 0.027	11.55 ± 0.16	299.1 ± 9.1	16.04 ± 0.48	81.99 ± 0.83	41.94 ± 0.49	37.74 ± 0.41
670	0.25	5.783 ± 0.182	0.3134 ± 0.0107	0.017	0.594 ± 0.051	0.371 ± 0.044	12.48 ± 0.25	285 ± 15	15.90 ± 0.81	81.67 ± 1.15	43.37 ± 0.68	41.13 ± 0.68
850	2.59	7.537 ± 0.038	0.1301 ± 0.0013	0.056	0.588 ± 0.020	0.476 ± 0.022	11.03 ± 0.16	157.6 ± 1.7	15.76 ± 0.26	82.41 ± 0.64	52.49 ± 0.40	53.95 ± 0.55
950	38.23	8.341 ± 0.042	0.0435 ± 0.0004	0.930	0.769 ± 0.007	0.550 ± 0.007	9.12 ± 0.03	106.9 ± 0.3	15.61 ± 0.05	83.83 ± 0.25	59.20 ± 0.15	64.29 ± 0.16
1090	59.49	8.364 ± 0.042	0.0418 ± 0.0004	1.46	0.773 ± 0.007	0.550 ± 0.005	9.07 ± 0.03	106.2 ± 0.3	15.56 ± 0.05	83.96 ± 0.25	59.30 ± 0.15	64.24 ± 0.16
1225	3.11	7.359 ± 0.037	0.1327 ± 0.0013	0.121	0.739 ± 0.022	0.510 ± 0.018	9.05 ± 0.08	105.3 ± 0.5	15.49 ± 0.16	83.18 ± 0.33	56.38 ± 0.30	60.05 ± 0.39
1440	0.23	1.780 ± 0.310	0.6777 ± 0.0246	0.012	0.669 ± 0.056	0.572 ± 0.073	9.85 ± 0.30	106.7 ± 1.5	15.55 ± 1.13	83.72 ± 1.14	51.59 ± 1.23	53.50 ± 2.09
1650	*0.06*			0.003	0.833 ± 0.222	0.464 ± 0.201	11.43 ± 0.76	109.5 ± 5.2	14.93 ± 4.96	82.78 ± 3.79	48.24 ± 3.21	56.21 ± 7.74
1769	0.21	7.866 ± 0.201	0.1707 ± 0.0093	0.009	0.561 ± 0.087	0.483 ± 0.101	16.10 ± 1.35	109.3 ± 2.4	16.07 ± 0.45	84.25 ± 2.16	46.44 ± 1.32	44.07 ± 1.69
Total	104.46	8.277 ± 0.041	0.0503 ± 0.0005	2.64	0.761 ± 0.005	0.544 ± 0.004	9.21 ± 0.03	111.0 ± 0.3	15.59 ± 0.05	83.81 ± 0.25	58.59 ± 0.15	63.25 ± 0.16
Axtell CV3 Diamond Separate (AF) 342 ± 3 μg												
350	14.90	8.701 ± 0.044	0.0388 ± 0.0004	0.370	0.737 ± 0.017	0.539 ± 0.011	10.77 ± 0.06	107.5 ± 0.3	15.53 ± 0.09	83.99 ± 0.30	59.60 ± 0.66	63.79 ± 0.93
440	15.75	8.710 ± 0.044	0.0370 ± 0.0004	0.308	0.763 ± 0.021	0.555 ± 0.011	10.59 ± 0.07	109.3 ± 0.5	15.42 ± 0.08	83.87 ± 0.34	59.37 ± 0.77	63.41 ± 1.10
670	35.32	8.830 ± 0.044	0.0360 ± 0.0004	0.553	0.764 ± 0.016	0.541 ± 0.009	10.11 ± 0.04	113.8 ± 0.3	15.46 ± 0.06	83.93 ± 0.25	60.43 ± 0.46	64.96 ± 0.67
850	28.19	8.766 ± 0.044	0.0362 ± 0.0004	0.363	0.789 ± 0.021	0.521 ± 0.010	9.77 ± 0.06	110.0 ± 0.5	15.51 ± 0.06	84.17 ± 0.34	61.19 ± 0.72	66.01 ± 1.02
950	31.34	8.463 ± 0.042	0.0366 ± 0.0004	0.427	0.774 ± 0.018	0.563 ± 0.013	9.64 ± 0.05	106.9 ± 0.3	15.51 ± 0.07	84.33 ± 0.30	62.03 ± 0.64	67.16 ± 0.89
1090	142.0	8.498 ± 0.042	0.0357 ± 0.0004	1.99	0.803 ± 0.006	0.552 ± 0.005	9.20 ± 0.03	104.8 ± 0.3	15.46 ± 0.05	84.04 ± 0.25	62.40 ± 0.16	68.33 ± 0.23
1225	317.6	8.501 ± 0.043	0.0365 ± 0.0004	7.08	0.807 ± 0.004	0.554 ± 0.003	9.08 ± 0.03	105.4 ± 0.3	15.50 ± 0.05	84.13 ± 0.25	62.49 ± 0.16	68.50 ± 0.17
1340	192.0	8.364 ± 0.042	0.0379 ± 0.0004	3.27	0.795 ± 0.004	0.561 ± 0.004	9.11 ± 0.03	106.5 ± 0.3	15.56 ± 0.05	84.06 ± 0.25	60.44 ± 0.15	66.30 ± 0.17

(Continued)

Appendix 1. (Continued)

Temp °C	^{22}Ne 10^{-8} cc/g	^{20}Ne/^{22}Ne	^{21}Ne/^{22}Ne	^{132}Xe 10^{-8} cc/g	^{124}Xe/^{132}Xe	^{126}Xe/^{132}Xe	^{128}Xe/^{132}Xe	^{129}Xe/^{132}Xe	^{130}Xe/^{132}Xe	^{131}Xe/^{132}Xe	^{134}Xe/^{132}Xe	^{136}Xe/^{132}Xe
1450	81.27	8.164 ± 0.041	0.0395 ± 0.0004	1.93	0.762 ± 0.006	0.540 ± 0.006	9.11 ± 0.05	107.4 ± 0.3	15.68 ± 0.05	83.94 ± 0.25	57.27 ± 0.16	62.51 ± 0.24
1580	23.77	7.872 ± 0.039	0.0419 ± 0.0004	0.934	0.776 ± 0.012	0.547 ± 0.015	8.94 ± 0.20	107.1 ± 0.4	15.65 ± 0.10	84.02 ± 0.36	57.72 ± 0.34	62.86 ± 0.45
1769	10.19	7.718 ± 0.039	0.0595 ± 0.0010	6.15	0.757 ± 0.004	0.544 ± 0.003	9.08 ± 0.03	106.9 ± 0.3	15.69 ± 0.05	83.94 ± 0.25	57.33 ± 0.14	62.50 ± 0.16
1800	0.509	7.685 ± 0.309	0.5038 ± 0.1426	2.18	0.754 ± 0.006	0.545 ± 0.005	9.29 ± 0.26	106.7 ± 0.3	15.61 ± 0.05	84.03 ± 0.25	57.51 ± 0.16	62.69 ± 0.21
Total	892.78	8.441 ± 0.042	0.0376 ± 0.0004	25.56	0.781 ± 0.004	0.549 ± 0.003	9.19 ± 0.03	106.5 ± 0.3	15.58 ± 0.05	84.03 ± 0.25	59.84 ± 0.18	65.34 ± 0.20
Acfer 214 CH HF-HCl Residue (AC) 406.3 ± 1.3 μg												
200	0.118	9.110 ± 0.444	0.0345 ± 0.0051	0.005	0.281 ± 0.233	0.316 ± 0.225	7.43 ± 0.90	93.5 ± 0.4	15.42 ± 0.94	78.41 ± 8.80	41.87 ± 1.73	37.81 ± 1.70
350	0.209	9.306 ± 0.258	0.0782 ± 0.0047	0.526	0.365 ± 0.011	0.342 ± 0.010	7.35 ± 0.05	99.4 ± 0.3	15.45 ± 0.06	79.94 ± 0.27	38.79 ± 0.17	33.10 ± 0.10
625	1.71	7.639 ± 0.070	0.0809 ± 0.0017	1.67	0.455 ± 0.006	0.400 ± 0.005	8.04 ± 0.03	105.2 ± 0.3	16.05 ± 0.05	81.40 ± 0.25	37.76 ± 0.09	31.48 ± 0.08
880	5.64	8.295 ± 0.041	0.0898 ± 0.0009	1.72	0.469 ± 0.006	0.410 ± 0.007	8.22 ± 0.03	104.4 ± 0.3	16.20 ± 0.05	82.05 ± 0.25	38.17 ± 0.10	31.84 ± 0.08
1100	17.02	7.782 ± 0.039	0.0515 ± 0.0005	3.18	0.481 ± 0.004	0.422 ± 0.005	8.32 ± 0.03	103.9 ± 0.3	16.27 ± 0.05	82.12 ± 0.25	39.20 ± 0.10	33.46 ± 0.08
1300	10.31	7.822 ± 0.039	0.0811 ± 0.0008	3.20	0.483 ± 0.005	0.415 ± 0.005	8.28 ± 0.03	103.7 ± 0.3	16.23 ± 0.05	81.90 ± 0.25	38.86 ± 0.10	33.28 ± 0.08
1495	3.08	7.370 ± 0.052	0.1374 ± 0.0022	1.50	0.490 ± 0.006	0.423 ± 0.007	8.25 ± 0.03	103.7 ± 0.3	16.18 ± 0.05	81.82 ± 0.25	39.06 ± 0.10	33.40 ± 0.08
1690	0.486	7.507 ± 0.193	0.1488 ± 0.0074	0.944	0.468 ± 0.007	0.407 ± 0.007	8.28 ± 0.05	103.7 ± 0.3	16.27 ± 0.07	82.11 ± 0.25	38.51 ± 0.11	32.47 ± 0.10
1769	0.20	8.544 ± 0.320	0.1142 ± 0.0081	0.702	0.471 ± 0.009	0.405 ± 0.009	8.28 ± 0.04	103.8 ± 0.3	16.40 ± 0.07	81.85 ± 0.25	38.46 ± 0.10	32.57 ± 0.10
Total	38.78	7.908 ± 0.040	0.0753 ± 0.0008	13.44	0.472 ± 0.002	0.411 ± 0.002	8.21 ± 0.02	103.8 ± 0.3	16.19 ± 0.05	81.83 ± 0.25	38.69 ± 0.10	32.83 ± 0.08
Acfer 214 CH Etched HF-HCl Residue (AD) 339.6 ± 0.6 μg												
200				*0.002*								
350	0.080	7.406 ± 0.767	0.305 ± 0.105	0.259	0.390 ± 0.019	0.323 ± 0.011	7.23 ± 0.07	99.3 ± 0.5	15.26 ± 0.13	78.92 ± 0.48	38.34 ± 0.23	33.06 ± 0.22
625	3.82	7.106 ± 0.053	0.0802 ± 0.0012	1.84	0.434 ± 0.005	0.394 ± 0.006	7.94 ± 0.04	107.1 ± 0.3	15.92 ± 0.05	81.62 ± 0.25	37.68 ± 0.09	31.40 ± 0.08
800	9.37	7.992 ± 0.040	0.0728 ± 0.0007	0.983	0.474 ± 0.010	0.395 ± 0.008	8.14 ± 0.04	105.0 ± 0.3	16.07 ± 0.07	82.27 ± 0.25	38.48 ± 0.10	31.99 ± 0.10
950	20.49	8.460 ± 0.042	0.0489 ± 0.0005	0.600	0.615 ± 0.013	0.473 ± 0.017	8.55 ± 0.07	104.5 ± 0.3	16.17 ± 0.07	83.04 ± 0.41	47.02 ± 0.16	45.34 ± 0.14
1120	24.99	7.774 ± 0.039	0.0465 ± 0.0005	0.597	0.666 ± 0.020	0.491 ± 0.014	8.88 ± 0.12	103.5 ± 0.5	16.21 ± 0.16	82.18 ± 0.55	51.55 ± 0.27	51.94 ± 0.20
1250	14.54	7.245 ± 0.036	0.0532 ± 0.0005	0.630	0.616 ± 0.011	0.476 ± 0.012	8.88 ± 0.09	104.9 ± 0.3	16.27 ± 0.06	83.01 ± 0.31	48.31 ± 0.20	48.20 ± 0.14
1395	0.988	3.253 ± 0.308	0.2352 ± 0.0100	0.224	0.495 ± 0.017	0.383 ± 0.016	8.30 ± 0.09	103.0 ± 0.5	16.50 ± 0.13	81.27 ± 0.54	38.18 ± 0.19	32.39 ± 0.18
1545	0.068		0.8566 ± 0.0791	0.178	0.445 ± 0.020	0.429 ± 0.022	8.41 ± 0.10	104.5 ± 0.5	16.44 ± 0.16	81.92 ± 0.40	38.02 ± 0.25	32.00 ± 0.29
1769	0.100	6.030 ± 0.807	0.3360 ± 0.0300	0.244	0.439 ± 0.016	0.414 ± 0.013	8.35 ± 0.10	103.6 ± 0.5	16.48 ± 0.16	82.44 ± 0.35	37.72 ± 0.23	31.56 ± 0.23
Total	74.45	7.782 ± 0.039	0.0575 ± 0.0006	5.55	0.507 ± 0.004	0.421 ± 0.004	8.26 ± 0.02	105.0 ± 0.3	16.08 ± 0.05	82.01 ± 0.25	41.59 ± 0.10	37.26 ± 0.09
Acfer 214 CH Diamond Separate (AF) 34.5 ± 1.0 μg												
200	1.16	9.521 ± 0.597	0.0242 ± 0.0074									
350	2.54	8.945 ± 0.255	0.0303 ± 0.0038	0.328	0.508 ± 0.125	0.442 ± 0.068	8.11 ± 0.27	110.5 ± 1.3	15.80 ± 0.34	85.13 ± 1.29	37.51 ± 0.71	31.72 ± 1.83
625	49.17	8.697 ± 0.043	0.0314 ± 0.0004	15.00	0.471 ± 0.006	0.412 ± 0.008	8.09 ± 0.04	109.1 ± 0.3	16.04 ± 0.07	82.50 ± 0.18	38.15 ± 0.09	31.71 ± 0.10
800	69.45	8.530 ± 0.043	0.0312 ± 0.0003	9.56	0.477 ± 0.012	0.423 ± 0.007	8.14 ± 0.05	104.7 ± 0.3	15.85 ± 0.05	82.34 ± 0.23	38.74 ± 0.16	32.67 ± 0.13
950	120.1	8.482 ± 0.042	0.0328 ± 0.0003	3.19	0.554 ± 0.020	0.438 ± 0.013	8.22 ± 0.08	103.9 ± 0.3	15.90 ± 0.09	83.29 ± 0.38	43.85 ± 0.18	40.79 ± 0.24
1200	257.7	8.402 ± 0.042	0.0351 ± 0.0004	2.33	0.740 ± 0.028	0.498 ± 0.021	8.84 ± 0.08	102.9 ± 0.3	15.56 ± 0.17	83.52 ± 0.47	59.12 ± 0.31	62.16 ± 0.27
1395	283.5	8.349 ± 0.042	0.0365 ± 0.0004	5.43	0.766 ± 0.016	0.550 ± 0.011	8.81 ± 0.07	104.5 ± 0.3	15.52 ± 0.08	83.54 ± 0.26	58.16 ± 0.22	62.39 ± 0.20
1769	242.4	8.218 ± 0.041	0.0379 ± 0.0004	12.37	0.708 ± 0.010	0.523 ± 0.012	8.86 ± 0.04	105.4 ± 0.3	15.75 ± 0.05	83.38 ± 0.22	55.27 ± 0.13	58.64 ± 0.14
Total	1026.08	8.379 ± 0.042	0.0354 ± 0.0004	48.20	0.585 ± 0.005	0.464 ± 0.005	8.42 ± 0.03	106.1 ± 0.3	15.84 ± 0.05	82.93 ± 0.25	46.30 ± 0.12	44.33 ± 0.11

Uncertainties on gas amounts are from counting statistics and do not include ~10% uncertainty from standard pipette. Coded as follows: Plain text, ≤10%; Italics, 10–25%; Parentheses, 25–100%. Weights refer to samples measured in the mass spectrometer.